Predicting the glass transition temperature and viscosity of secondary organic material using molecular composition

Wing-Sy Wong DeRieux[1§], Ying Li[1§], Peng Lin[2], Julia Laskin[2], Alexander Laskin[2], Allan K. Bertram[3], Sergey A. Nizkorodov[1], and Manabu Shiraiwa[1*]

[1] Department of Chemistry, University of California, Irvine, CA 92697-2025, USA

[2] Department of Chemistry, Purdue University, West Lafayette, IN 47907-2084, USA

[3] Department of Chemistry, University of British Columbia, Vancouver, BC V6T 1Z1, Canada

[§] These authors contributed equally to this work.

[*]Correspondence to: M. Shiraiwa (m.shiraiwa@uci.edu)

Submitted to Atmospheric Chemistry and Physics (ACP)

Abstract:

Secondary organic aerosols (SOA) account for a large fraction of submicron particles in the atmosphere. SOA can occur in amorphous solid or semi-solid phase states depending on chemical composition, relative humidity (RH), and temperature. The phase transition between amorphous solid and semi-solid states occurs at the glass transition temperature (T_g). We have recently developed a method to estimate T_g of pure compounds containing carbon, hydrogen, and oxygen atoms (CHO compounds) with molar mass less than 450 g mol^{-1} based on their molar mass and atomic O:C ratio. In this study, we refine and extend this method for CH and CHO compounds with molar mass up to ~1100 g mol^{-1} using the number of carbon, hydrogen, and oxygen atoms. We predict viscosity from the T_g-scaled Arrhenius plot of fragility (viscosity vs. T_g/T) as a function of the fragility parameter D. We compiled D values of organic compounds from literature, and found that D approaches a lower limit of ~10 (+/- 1.7) as the molar mass increases. We estimated viscosity of α-pinene and isoprene SOA as a function of RH by accounting for hygroscopic growth of SOA and applying the Gordon-Taylor mixing rule, reproducing previously published experimental measurements very well. Sensitivity studies were conducted to evaluate impacts of T_g, D, hygroscopicity parameter (κ), and the Gordon-Taylor constant on viscosity predictions. Viscosity of toluene SOA was predicted using the elemental composition obtained by high-resolution mass spectrometry (HRMS), resulting in a good agreement with the measured viscosity. We also estimated viscosity of biomass burning particles using the chemical composition measured by HRMS with two different ionization techniques: electrospray ionization (ESI) and atmospheric pressure photoionization (APPI). Due to differences in detected organic compounds and signal intensity, predicted viscosities at low RH based on ESI and APPI measurements differ by 2-5 orders of magnitude. Complementary

measurements of viscosity and chemical composition are desired to further constrain RH-dependent viscosity in future studies.

1. Introduction

Secondary organic aerosols (SOA) account for a large fraction of submicron particles in the atmosphere and they play an important role in climate, air quality and public health (Goldstein and Galbally, 2007; Jimenez et al., 2009). Traditionally, SOA particles were assumed to be liquid with dynamic viscosity η below 10^2 Pa s, but a number of recent studies have shown that they can also adopt amorphous semi-solid ($10^2 \leq \eta \leq 10^{12}$ Pa s), or glassy solid ($\eta > 10^{12}$ Pa s) states, depending on chemical composition and temperature (Zobrist et al., 2008; Koop et al., 2011; Huang et al., 2018; Reid et al., 2018). The phase state is also strongly affected by relative humidity, as water can act as a plasticizer to lower viscosity (Mikhailov et al., 2009). Ambient and laboratory-generated SOA particles have been observed to bounce off the smooth hard surface of an inertial impactor at low RH, implying a non-liquid state (Virtanen et al., 2010; Saukko et al., 2012; Bateman et al., 2015; Jain and Petrucci, 2015), whereas predominantly biogenic SOA particles in the Amazon basin did not bounce off the impactor surface at high RH, implying they are primarily liquid (Bateman et al., 2016). Upon dilution or heating, SOA particles were observed to evaporate unexpectedly slowly (Cappa and Wilson, 2011; Vaden et al., 2011), and recent modeling studies have evaluated the contributions of low diffusivity and volatility to slow evaporation rates (Roldin et al., 2014; Yli-Juuti et al., 2017). Measurements of viscosity of SOA bulk material derived from oxidation of α-pinene (Renbaum-Wolff et al., 2013; Zhang et al., 2015; Hosny et al., 2016), limonene (Hinks et al., 2016), isoprene (Song et al.,

2015), and toluene (Song et al., 2016a) have confirmed that SOA particles adopt a wide range of viscosities.

The particle phase state has been shown to affect gas uptake and chemical transformation of organic compounds due to kinetic limitations of bulk diffusion (Shiraiwa et al., 2011; Abbatt et al., 2012; Kuwata and Martin, 2012; Zhou et al., 2013; Slade and Knopf, 2014; Arangio et al., 2015; Davies and Wilson, 2015; Wang et al., 2015; Berkemeier et al., 2016; Marshall et al., 2016; Liu et al., 2018; Pratap et al., 2018; Zhang et al., 2018). Molecular motion can be hindered in a highly viscous matrix, slowing down photochemical reactions in particles (Lignell et al., 2014; Hinks et al., 2016). Water diffusion can be still fast even in an amorphous solid matrix under room temperature, but it can be hindered significantly under low temperatures (Mikhailov et al., 2009; Zobrist et al., 2011; Bones et al., 2012; Berkemeier et al., 2014; Price et al., 2014), affecting homogeneous vs. heterogeneous ice nucleation pathways (Murray et al., 2010; Wang et al., 2012a; Wang et al., 2012b; Baustian et al., 2013; Schill and Tolbert, 2013; Berkemeier et al., 2014; Schill et al., 2014; Lienhard et al., 2015; Ignatius et al., 2016; Knopf et al., 2018). Despite the substantial implications of the SOA particle phase state, its effects on gas-particle interactions have not yet been considered explicitly in current climate and air quality models (Shrivastava et al., 2017).

Partitioning of semi-volatile compounds into viscous particles may result in kinetically-limited growth in contrast to quasi-equilibrium growth (Perraud et al., 2012; Shiraiwa and Seinfeld, 2012; Booth et al., 2014; Zaveri et al., 2014; Mai et al., 2015; Liu et al., 2016), which also affects the evolution of particle size distribution upon SOA growth (Shiraiwa et al., 2013; Zaveri et al., 2018). Chamber experiments probing mixing timescales of SOA particles derived by oxidation of various precursors such as isoprene, terpene, and toluene have observed strong

kinetic limitations at low RH, but not at moderate and high RH (Loza et al., 2013; Ye et al., 2016; Ye et al., 2018). Gorkowski et al. (2017) did not observe significant diffusion limitations for glycerol and squalene in α-pinene SOA. Quasi-equilibrium versus kinetically-limited or non-equilibrium SOA growth remains an open issue and warrants further investigations.

Group contribution methods have been used to predict the viscosities of pure compounds when the functionality and molecular structure are known (Sastri and Rao, 1992; Rothfuss and Petters, 2017). Song et al. (2016) showed that estimations from group contribution approaches combined with either nonideal or ideal mixing reproduced the RH-dependent trends particularly well for the alcohol, di-, and tricarboxylic acid systems with viscosity of up to 10^4 Pa s. By contrast, model calculations overestimated the viscosity of more viscous compounds including mono-, di-, and trisaccharides by many orders of magnitude (Song et al., 2016b). A recent study compiled viscosity of organic compounds with atmospherically relevant functional groups, investigating the influence of the number and location of functional groups on viscosity (Rothfuss and Petters, 2017). These studies provide important insights in estimating the viscosity of individual organic compounds.

Particle phase state can be characterized by a glass transition temperature (T_g), which is a characteristic temperature representing a non-equilibrium phase transition from a glassy solid state to a semi-solid state as the temperature increases (Koop et al., 2011). Recently, we have developed a method to estimate T_g of pure organic compounds comprised of carbon, hydrogen, and oxygen (CHO compounds) with molar mass less than 450 g mol^{-1} based on their molar mass and atomic O:C ratio (Shiraiwa et al., 2017). It has been applied successfully in a global chemistry climate model to predict T_g and the phase state of atmospheric SOA, which indicated that SOA particles are mostly liquid or semi-solid in the planetary boundary layer, while they

should be glassy in the middle and upper troposphere (Shiraiwa et al., 2017). A recent study provided a consistent result, suggesting that mixing timescales of organic molecules within SOA are often < 1 h in a global planetary boundary layer (Maclean et al., 2017).

It has been shown that SOA particles contain oligomeric compounds with molar masses higher than 450 g mol^{-1} (Gao et al., 2004; Tolocka et al., 2004; Nizkorodov et al., 2011; Nozière et al., 2015), which makes the previously developed parameterization incomplete. In this study, we extend the parameterization of T_g to higher molar mass compounds, and apply it to high-resolution mass spectrometry data for toluene SOA and biomass burning particles. The Arrhenius approach and the Gordon-Taylor mixing rules were applied to estimate viscosity of SOA bulk materials to compare with the literature reported viscosity measurements. This method will be useful for estimations of viscosity of organic particles, for which high-resolution mass spectra are available. It can also be applied in global or regional models to evaluate impacts of the particle phase state on the role of SOA in climate and air quality.

2. Parameterization development

2.1 Glass transition temperature

Figure 1a shows the dependence of T_g on the molar mass (M) of organic compounds. Solid markers represent measured T_g of 258 CHO compounds (Koop et al., 2011; Dette et al., 2014; Rothfuss and Petters, 2017), while open markers represent 654 CHO compounds in SOA (Shiraiwa et al., 2014). Markers are color-coded by atomic O:C ratio. Their melting points (T_m) were estimated by the Estimation Programs Interface (EPI) Suite software version 4.1 (US-EPA, 2012) and their T_g were estimated using the Boyer-Kauzmann rule: $T_g = g \cdot T_m$ with $g = 0.7$ (Koop et al., 2011; Shiraiwa et al., 2017). This rule can provide good estimates of T_g, as has been

validated in previous work (Koop et al., 2011) and also shown in Fig. A2(a). A subset of data shown in Figure 1 was originally published in Shiraiwa et al. (2017) for compounds with $M <$ 450 g mol^{-1}. This version of the figure has been updated to include a number of experimentally measured T_g values of larger compounds with M up to 1153 g mol^{-1}, including aliphatic compounds containing OH and/or COOH groups. Specifically, data for 76 aliphatic alcohols, 39 carbohydrates and their derivatives, 4 carboxylic acids, and 4 hydroxy acids, as compiled by Rothfuss and Petters (2017), have been added to Figure 1. Eight of these compounds are carbohydrates with $M > 450$ g mol^{-1}. These updates are critical for reliable parameterization of T_g based on M. When M increases above ~500 g mol^{-1}, the slope of T_g decreases, making it challenging to extrapolate the low-M data from the original Shiraiwa et al. (2017) study to higher M values. When M increases to ~1000 g mol^{-1}, the corresponding T_g appears to level at around 420 K.

Such dependence on M has been described for polymers with the Fox-Flory equation: $T_g(M) = T_{g,\infty} - \frac{K_m}{M}$ (Fox Jr and Flory, 1950), where K_m is a constant and $T_{g,\infty}$ is the asymptotic value of T_g specific to the polymer. We conducted a literature search and found that most of the reported $T_{g,\infty}$ values fell below ~500 K (Fox Jr and Flory, 1950; Onder et al., 1972; Montserrat and Colomer, 1984; Polymer handbook, 1999; Papadopoulos et al., 2004; Matsushima et al., 2017). The Fox-Flory equation works very well for high molar mass compounds and is also generally applicable to smaller compounds (Koop et al., 2011), as supported by an approximately linear dependence of T_g on the inverse molar mass in Fig. A1(a). Figure 1b plots the values of T_g as a function of the atomic O:C ratio of organic molecules. Figures 1a and 1b clearly demonstrate that T_g depends primarily on the molar mass with a weak dependence on the atomic O:C ratio.

A parameterization for T_g calculation based on the molar mass and atomic O:C ratio was developed in our recent work, which is applicable to CH and CHO compounds with $M < 450$ g mol^{-1} (Shiraiwa et al., 2017):

$$T_g = A + BM + C^2M^2 + D\,(O{:}C) + E\,M\,(O{:}C) \quad (1)$$

where A = –21.57 (±13.47) [K], B = 1.51 (±0.14) [K mol g^{-1}], C = -1.7×10^{-3} ($\pm3.0\times10^{-4}$) [K mol^2 g^{-2}], D = 131.4 (±16.01) [K] and E = –0.25 (±0.085) [K mol g^{-1}], respectively. These values were obtained by fitting the measured T_g of 179 CH and CHO compounds with $M < 450$ g mol^{-1} with multi-linear least squares analysis. Note that application of Eq. (1) may provide unreasonable T_g values for compounds with $M > 500$ g mol^{-1} because it does not account for the strong curvature in the T_g vs. M dependence shown in Figure 1a.

In this study we have developed an improved parameterization to predict T_g of CH and CHO compounds using the number of carbon (n_C), hydrogen (n_H), and oxygen (n_O) that can also be applied to higher molar mass compounds. Motivated by a good correlation between T_g and volatility (Fig. 1a in Shiraiwa et al., (2017)), we use an equation with a similar formulation to the equation used to predict the saturation mass concentration or volatility (Donahue et al., 2011; Li et al., 2016):

$$T_g = (n_C^0 + ln(n_C))\,b_C + ln(n_H)\,b_H + ln(n_C)\,ln(n_H)\,b_{CH} + ln(n_O)\,b_O + ln(n_C)\,ln(n_O)\,b_{CO} \quad (2)$$

where n_C^0 is the reference carbon number, b_C, b_H and b_O denote the contribution of each atom to T_g, and b_{CH} and b_{CO} are coefficients that reflect contributions from carbon-hydrogen and carbon-oxygen bonds, respectively. These values were obtained by fitting the measured T_g of 42 CH compounds and 258 CHO compounds with multi-linear least squares analysis with 68% prediction and confidence intervals. The best-fit parameters are summarized in Table 1.

176 Note that the evaluation dataset used to derive Eq. (2) contains CH compounds with $M <$
177 260 g mol^{-1} (see Fig. A2b for comparison of measured and predicted T_g). Thus, the application of
178 Eq. (2) to higher molar mass compounds may require further investigations when measured T_g
179 for higher molar mass compounds becomes available. We plan to continue to refine our method
180 as additional glass transition data on high molar mass compounds become available. Figure 1c
181 shows that the T_g values predicted using Eq. (2) are in good agreement with the T_g values
182 measured in experiments (see also Fig. A1(b)) or estimated by the Boyer-Kauzmann rule as
183 indicated by the high correlation coefficient of 0.95. T_g of individual compounds can be
184 predicted within ±21 K as indicated by the prediction band (dotted lines in Fig. 1c); however,
185 this uncertainty may be much smaller for multicomponent SOA mixtures under ideal mixing
186 conditions as indicated in the confidence band (dashed lines, almost overlapping with the 1:1
187 line).

188 These results are noteworthy given that the parameterization (Eq. 2) does not consider
189 either explicit molecular structures or functional groups. Previous studies have shown that T_g can
190 be especially sensitive to the number of OH groups, which interact strongly through hydrogen
191 bonding. For example, Nakanishi et al., (2011) found a direct relationship between T_g and the
192 number of hydroxyl groups in a molecule for sugar alcohols; T_g increases as the number of OH
193 groups increases. They reported that the correlation between T_g and the number of OH groups
194 was much stronger than the correlation between T_g and the number of carbons in a molecule.
195 Such a trend is implicitly included in Eq. (1) and (2), which contain the O:C ratio and number of
196 oxygen atoms as parameters, respectively. Recently, Rothfuss and Petters (2017) showed an
197 approximately linear relationship between the number of OH groups and T_g for compounds with
198 up to eight OH groups. Grayson et al. (2017) showed that addition of hydroxyl functional groups

199 increases viscosity, a conclusion supported by both the experimental data and quantitative
200 structure-property relationship model. The correlation between T_g and the number of carbon
201 atoms is consistent with the free volume theory, in which molecular motion is restricted by the
202 difference between the space required for a molecule to vibrate versus the space in which the
203 molecule resides (i.e., the free volume) (White and Lipson, 2016). The correlation between T_g
204 and the number of OH groups is more consistent with the topological constraint theory, where
205 the primary influence is the three dimensional structure of the molecule as determined by
206 molecular bonds and hydrogen-bonding networks (Nakanishi and Nozaki, 2011; van der Sman,
207 2013). Future experiments targeting more comprehensive T_g data, especially for higher molar
208 mass compounds, would lead to further refinements of our T_g parameterizations.

209 Comparing Eq. (1) and (2), the two parameterizations give similar performance for
210 compounds with $M < 450$ g mol^{-1} as shown in Fig. A2c. The statistical measures of correlation
211 coefficient (R), mean bias (MB), and root mean square error (RMSE) are 0.93, –6.45 K, and
212 25.64 K, respectively, for the performance of Eq. (1), while for Eq. (2), they are 0.95, 3.15 K,
213 and 21.11 K, respectively. It should be noted again that Eq. (1) cannot be used to predict T_g for
214 compounds with $M > 450$ g mol^{-1}. For example, T_g of stachyose ($M = 667$ g mol^{-1}) predicted by
215 Eq. (1) is 198 K, while that by Eq. (2) is 394 K, which agrees much better with the measured
216 mean T_g of 396 K (Rothfuss and Petters, 2017). Eq. (2) is more flexible than Eq. (1) and can be
217 potentially expanded to include compounds containing hetero-atoms (e.g., nitrogen or sulfur),
218 once substantial sets of experimental values of T_g for such compounds become available.
219 Regarding the application in air quality and climate models, Eq. (1) can be applied in the
220 volatility basis set (VBS) (Donahue et al., 2006; Donahue et al., 2011) and the molecular
221 corridor approach (Shiraiwa et al., 2014; Li et al., 2016) to predict the T_g of SOA particles

(Shiraiwa et al., 2017), while the new parameterization may be suitable for coupling with the statistical oxidation model which characterizes the SOA evolution as a function of n_C and n_O (Cappa and Wilson, 2012; Jathar et al., 2015).

These parameterizations (Eqs. 1, 2) calculate T_g based on the elemental composition of organic compounds. SOA particles contain a number of organic compounds as well as a variable amount of liquid water, which has low T_g (136 K) and can act as a plasticizer (Mikhailov et al., 2009; Koop et al., 2011). Under humid conditions, SOA particles take up water by hygroscopic growth in response to RH, lowering T_g and viscosity of SOA particles. Estimations of T_g for SOA-water mixtures were discussed by Shiraiwa et al. (2017), who applied the Gordon-Taylor equation validated for a wide range of mixtures of organics, polymer, and water (Roos, 1993; Hancock and Zografi, 1994; Zobrist et al., 2008; Dette et al., 2014; Dette and Koop, 2015). Briefly, T_g of mixtures of SOA compounds under dry conditions ($T_{g,org}$) were calculated assuming the Gordon-Taylor constant (k_{GT}) of 1 (Dette et al., 2014): $T_{g,org} = \sum_i w_i T_{g,i}$, where w_i is the mass fraction of organic compound i, which can be derived using mass concentrations of SOA products. The Gordon-Taylor equation can also be applied to calculate T_g of organic-water mixtures considering the mass fraction of organics (w_{org}) in SOA particles (Koop et al., 2011):

$$T_g(w_{org}) = \frac{(1-w_{org})T_{g,w} + \frac{1}{k_{GT}} w_{org} T_{g,org}}{(1-w_{org}) + \frac{1}{k_{GT}} w_{org}} \quad (3)$$

w_{org} can be calculated using the mass concentrations of water (m_{H_2O}) and SOA (m_{SOA}) as $w_{org} = m_{SOA} / (m_{SOA} + m_{H_2O})$. m_{H_2O} can be estimated using the effective hygroscopicity parameter (κ) (Petters and Kreidenweis, 2007):

$$m_{H2O} = \frac{\kappa \rho_w m_{SOA}}{\rho_{SOA}\left(\frac{1}{a_w} - 1\right)} \quad (4)$$

The density of water (ρ_w) is 1 g cm^{-3}, the density of SOA particles (ρ_{SOA}) is assumed to be 1.2 g cm^{-3} (Kuwata et al., 2012), m_{SOA} is the total mass concentrations of SOA, and a_w is the water activity calculated as a_w = RH/100. Pajunoja et al. (2015) found that water uptake in subsaturated conditions is inhibited until RH is high enough for dissolution of water in SOA particles with relatively low O:C ratios. As oxidation of SOA increases, solubility of water increases and dissolution occurs at lower RH values. In both cases, the use of subsaturated hygroscopicity measurements was supported.

2.2 Viscosity

Temperature dependence of viscosity (η) was predicted using the modified Vogel-Tammann-Fulcher (VTF) equation (Angell, 1991):

$$\eta = \eta_\infty e^{\frac{T_0 D}{T - T_0}} \quad (5)$$

where η_∞ is viscosity at infinite temperature; T_0 is the Vogel temperature; T is the ambient temperature. The fragility parameter, D, characterizes how rapidly the dynamics of a material slow down as T approaches T_g, reflecting to what degree the temperature dependence of the viscosity deviates from Arrhenius behavior. When T is close to T_g ($T_g/T \approx 1$), smaller D values indicate that viscosity is sensitive to temperature change (fragile behavior); while larger D values indicate that viscosity is less sensitive to temperature change (strong or Arrhenius behavior).

Assuming η_∞=10^{-5} Pa s (Angell, 1991):

$$\log \eta = -5 + 0.434 \frac{T_0 D}{T - T_0} \quad (6)$$

When $T = T_g$, η = 10^{12} Pa s, which leads to (Angell, 1991; Angell, 2002):

$$T_0 = \frac{39.17\, T_g}{D + 39.17} \quad (7)$$

As can be seen in Eq. (5), both T_g and D are required to calculate η from Eq. (4) at a given temperature.

Figure 2 shows the T_g-scaled Arrhenius plot of fragility (viscosity versus T_g/T) referred to as an Angell plot (Angell, 1995). D values of organic compounds are typically in the range of ~5–30 (Angell, 1997). To estimate D values that could be applied to SOA compounds, we compiled measured fragility values. Fragility was often measured in the form of the fragility steepness index (m), which represents the slope of the Arrhenius plot at the point where $T = T_g$ (Boehmer et al., 1993). Compounds with lower m exhibit higher D values, indicating stronger glass formers. The measured m of 95 organic compounds are included in the Supplement. m can be converted to D using the following equation (see the full derivation of this equation in Appendix A):

$$D = \frac{665.89}{m-17} \quad (8)$$

Figure 3 shows the measured D as a function of (a) molar mass and (b) atomic O:C ratio of organic molecules. The molar mass exerts a stronger effect on fragility, while there is little dependence of D on the O:C ratio. As molar mass increases, D approaches a lower limit of 10.3 (± 1.7), consistent with the value of 10 used in our recent study (Shiraiwa et al., 2017). To evaluate the impact of the variations of D on viscosity prediction, sensitivity calculations were conducted as described in Sect. 3.

Besides the VTF equation, another commonly used equation for describing the temperature dependence of viscosity is the Williams-Landel-Ferry (WLF) equation: $\log\frac{\eta(T)}{\eta(T_g)} = \frac{-C_1(T-T_g)}{C_2+(T-T_g)}$, where empirical parameters C_1 and C_2 are adopted as 17.44 and 51.6 K, respectively (Williams et al., 1955; Schill and Tolbert, 2013; Wang et al., 2015). The two equations are

mathematically equivalent, both defined with respect to a reference temperature, and their parameters are related through $C_1 = \frac{DT_0}{2.303(T_g - T_0)}$ and $C_2 = T_g - T_0$. For the WLF equation, T_g is the reference temperature and there is a linear dependence assumed between temperature and free volume (O'Connell and McKenna, 1999; Huang and McKenna, 2001; Metatla and Soldera, 2007). For the VTF equation, the reference is the Vogel temperature (T_0)–a hypothetical temperature at which all non-vibrational motion ceases and viscosity becomes infinite and the theoretical foundation of the VTF equation includes both thermodynamic and kinetic considerations (O'Connell and McKenna, 1999; Huang and McKenna, 2001; Metatla and Soldera, 2007). The calculations of viscosity in this study are based mainly on the VTF equation and the difference between calculated results from the two equations will be briefly discussed in the following section.

3. Comparison of predicted viscosity with measurements

3.1. SOA formed from α–pinene and isoprene

The purpose of this section is to demonstrate that viscosity of SOA material can be predicted over a broad range of RH values from four parameters: T_g of dry SOA ($T_{g,org}$), fragility (D), hygroscopicity (κ), and the Gordon-Taylor constant for mixing SOA and water (k_{GT}). Viscosity of α-pinene SOA has been measured as a function of RH by several groups using multiple experimental techniques as shown in Fig. 4(a) (Abramson et al., 2013; Renbaum-Wolff et al., 2013; Kidd et al., 2014; Pajunoja et al., 2014; Bateman et al., 2015; Zhang et al., 2015; Grayson et al., 2016). The wide range of experimentally measured viscosities reported for α-pinene SOA, particularly from 30-60% RH is most likely a consequence of the different experimental approaches, mass loadings and O:C ratios for each experiment. For instance,

Grayson et al. (2016) used mass loadings of 121 to 14000 μg m^3 and observed that viscosity decreased as mass loading increased. Higher mass loadings would lead to greater partitioning of semi-volatile and lower molar mass compounds into the particle phase, which would lead to the decrease of T_g and viscosity of the resulting SOA mixture. They concluded that their results should be considered a lower limit for viscosity of α-pinene SOA in the atmosphere. It should also be noted that the viscosity measurements from Renbaum-Wolff et al. (2013) were for the water-soluble portion of the SOA. These datasets suggest that viscosity of α-pinene SOA approaches very high values (~>10^8 Pa s) below 20-30% RH and decreases with an increase in RH reaching a value of ~10 Pa s at 80% RH. As can be seen in Fig. 4(b), isoprene SOA is less viscous with $\eta < 10^6$ Pa s even under dry conditions, undergoing a phase transition from a semi-solid phase to a liquid phase at ~55% RH (Bateman et al., 2015; Song et al., 2015).

The solid lines with the shaded areas in Figure 4 are viscosity values predicted using $T_{g,org}$, D, κ, k_{GT}. $T_{g,org}$ values were adopted by Berkemeier et al. (2014) who estimated $T_{g,org}$ with the Boyer-Kauzmann rule using the melting point of representative SOA oxidation products. Note that Eq. (1) or (2) were not used to estimate $T_{g,org}$, which should be done in future studies by obtaining their elemental composition using high resolution mass spectrometry. For α-pinene, $T_{g,org}$ was assumed to be 278 K corresponding to an O:C ratio of 0.5 (Berkemeier et al., 2014), which is a typical O:C ratio of α-pinene SOA (Aiken et al., 2008; Chen et al., 2011; Putman et al., 2012).

The $T_{g,org}$ selected for isoprene SOA was 255 K, corresponding to the O:C ratio of 0.6. Although no measurements of the O:C ratio for the experimental isoprene SOA data were reported, Song et al. (2015) estimated O:C of 0.64-1.1 based on literature values. As O:C ratios are useful in estimating $T_{g,org}$, we encourage the measurement of the O:C ratio of SOA when

conducting viscosity measurements. In contrast to α-pinene SOA, there are limited viscosity measurements for isoprene SOA. While the predicted viscosity is consistent with the experimental data, comparison of our model predictions to additional measurements is strongly recommended. Song et al. (2015) prepared their samples in a potential aerosol mass (PAM) reactor while those investigated by Bateman et al. (2015) were generated in a smog chamber. It has been suggested that under ambient conditions, the majority of isoprene-derived SOA can be derived through heterogeneous interactions with acidic sulfate particles forming oligomers (Lin et al., 2013; Surratt et al., 2010; Gaston et al., 2014), which may increase viscosity. Further studies are warranted to compare laboratory-generated and ambient isoprene SOA, and to investigate the effect of the acidic seed on the viscosity.

For both α-pinene and isoprene SOA, D was set to 10 based on the analysis presented in Fig. 3(a). κ was set to 0.1 based on field and laboratory measurements (Gunthe et al., 2009; Lambe et al., 2011b; Pajunoja et al., 2014; Petters et al., 2017) and k_{GT} was assumed to be 2.5 (Zobrist et al., 2008; Koop et al., 2011). Using these parameters, the predicted viscosities match well the magnitude and the RH-dependence of the measured viscosity of α-pinene and isoprene SOA. Figure 4 also shows predicted viscosities (dotted lines) using the WLF equation, which shows similar values as the VTF equation, but slightly underestimates the viscosity of α-pinene SOA at low RH and overestimates the viscosity of isoprene SOA at high RH.

Sensitivity studies were conducted to examine the effects of $T_{g,org}$, D, κ and k_{GT}, on the calculated viscosity. In these studies, $T_{g,org}$ of α-pinene and isoprene SOA were varied within 229-328 K and 255-316 K, respectively, representing $T_{g,org}$ of different oxidation states (Berkemeier et al., 2014). D was varied between 5 and 30, which is the range characteristic for organic compounds (see Fig. 3a). κ of 0.05-0.15 were used for α-pinene and isoprene SOA

356 (Lambe et al., 2011b; Pajunoja et al., 2015). For the Gordon-Taylor constant, values of 2.5±1.5
357 were considered (Zobrist et al., 2008; Koop et al., 2011; Dette et al., 2014; Dette and Koop,
358 2015).

359 The effect of varying each parameter on the calculated viscosity of α-pinene SOA is
360 illustrated in Fig. 5. Variations of ±50 K in $T_{g,org}$ result in 3-6 orders of magnitude difference in
361 calculated values at dry conditions, indicating that $T_{g,org}$ is a critical parameter for viscosity
362 estimations. Decreasing D from 10 to 5 led to a decrease of calculated values by more than one
363 order of magnitude. The calculated results were within the upper limit of measurements when
364 increasing D from 10 to 20, and the predicted values were only slightly enhanced when further
365 increasing D from 20 to 30. Calculated values with variations in κ from 0.05 to 0.15 and k_{GT}
366 from 1.0 to 4.0 were all within the measured ranges.

367 For isoprene SOA, an increase of $T_{g,org}$ to 287 K, which represents a higher oxidation
368 state (Berkemeier et al., 2014), led to calculated values to be several orders of magnitude higher
369 than the upper limit of measurements (Fig. 6a). When $T_{g,org}$ reaches 316 K, isoprene SOA can
370 occur as a solid for RH lower than ~40%. Compared to α-pinene SOA, a variation in D has a
371 larger effect on the calculated viscosity (Fig. 6b). For a range of 5 - 30 for D, calculations with
372 the D value of 10 agreed well with the measurements, while other D values resulted in calculated
373 viscosity outside of the measured ranges. Figures 6c and 6d show that decreasing κ and k_{GT}
374 below the reference values, the predictions overestimate the measured η by one or two orders of
375 magnitude. The latter is most evident at RH > 60%, where the calculated values were higher than
376 the upper limit of measurements. Modeling results with κ and k_{GT} increasing to 0.15 and 4.0,
377 respectively, were within the lower limit of measurements.

The above comparison between the measured and predicted viscosity demonstrates that the method described in this study can reproduce reasonably well the measured RH-dependent viscosity of SOA formed from α-pinene and isoprene. The sensitivity calculations showed that $T_{g,org}$ contributed the most to the uncertainty in the viscosity estimates. Previous studies have shown that the experimental conditions such as particle mass concentrations (Grayson et al., 2016) and RH upon SOA formation (Kidd et al., 2014; Hinks et al., 2018) can impact chemical composition of SOA and hence the phase state and viscosity. Further efforts to constrain the uncertainties are needed both in experiments and parameterizations.

3.2. SOA formed from toluene

In this and the following sections, we examine the feasibility of calculating the value of $T_{g,org}$ from mass spectrometry data on SOA. Hinks et al. (2017) measured the elemental composition of toluene SOA using nanospray desorption electrospray ionization high-resolution mass spectrometry (nano-DESI-HRMS) (Roach et al., 2010a, b). Toluene SOA were formed by OH photooxidation in an aerosol smog chamber at <2% RH (mass loading = 23 μg m^{-3}) and 75% RH (mass loading = 8 μg m^{-3}) to investigate the effect of RH on the chemical composition of toluene SOA formed under low-NO_x conditions. Measurements revealed a significant reduction in the fraction of oligomers present in toluene SOA generated under high RH conditions compared to SOA generated under low RH conditions (Hinks et al., 2017). The detected molar mass of individual oxidation products spanned a range of 102 - 570 g mol^{-1} at high RH, which increased up to 726 g mol^{-1} at low RH.

Figure 7(a) shows the interdependence of glass transition temperature, volatility, and molar mass of the detected toluene SOA compounds. Glass transition temperatures were

calculated using Eq. (2). Saturation mass concentrations or volatilities of detected compounds were estimated from the elemental composition by using the parameterization of Li et al. (2016). The analysis is based on the molecular corridor approach—a two-dimensional framework of volatility and molar mass of SOA components constrained by boundary lines of low and high atomic O:C ratio, corresponding to *n*-alkanes (C_nH_{2n+2}, O:C = 0) and sugar alcohols ($C_nH_{2n+2}O_n$, O:C = 1), respectively (Shiraiwa et al., 2014; Li et al., 2016). The toluene SOA constituents are well constrained by the molecular corridor and T_g are higher for compounds with higher molar mass and lower volatility.

Eq. (1) was used to calculate T_g for individual compounds with $M < 450$ g mol^{-1}, while excluding compounds with molar mass higher than 450 g mol^{-1}. This approach was deemed reasonable as such high molar mass compounds account for < 10% of all toluene SOA products formed at low RH, and for < 2% formed at high RH. Eq. (2) was used to calculate T_g for all the detected compounds. T_g of dry toluene SOA ($T_{g,org}$) was then computed using the Gordon-Taylor approach with $k_{GT} = 1$ (Sect. 2.1). The relative mass concentrations of individual components were assumed to be proportional to their relative abundance in the nano-DESI-HRMS spectrum. This assumption has a number of caveats (Bateman et al., 2012; Nguyen et al., 2013), and as we will see below, it results in deviations between the predicted and measured viscosity. Table 2 summarizes the results of such calculations, showing that the $T_{g,org}$ by Eq. (1) – excluding high molar mass compounds – is about 10 K lower as compared to $T_{g,org}$ by Eq. (2). $T_{g,org}$ at low RH is predicted to be higher than $T_{g,org}$ at high RH, which results from a lower abundance of high molar mass compounds observed at high RH. This trend is consistent with Kidd et al. (2014), who showed that SOA material formed under dry conditions is more viscous than that formed under wet conditions.

Figure 7(b) shows the predicted viscosity of toluene SOA as a function of RH, as compared to the measured viscosity of toluene SOA formed in an oxidation flow reactor at 13% RH (Song et al., 2016a). Indirect viscosity measurements are also included in shaded boxes (Bateman et al., 2015; Li et al., 2015). Lines with shaded areas are calculated viscosities using $T_{g,org}$ as described above. κ was assumed to be 0.25 based on laboratory measurements (Lambe et al., 2011a; Hildebrandt Ruiz et al., 2015). To achieve good fit, D was set to 13 and k_{GT} was assumed to be 3.0 (Dette et al., 2014). Estimations with Eq. (1) match the measured viscosity values very well over the entire RH range. Predictions with Eq. (2) overestimated the measurements by one or two orders of magnitude at moderate RH between 30% and 50%, while they agreed with the measurements derived at RH $\geq$ 60% and at the dry conditions.

There are several possible reasons for the difference between the measurements and predictions. First, the relative abundance of high molar mass compounds observed in HRMS measurements may be overestimated, as high molar mass compounds tend to have higher (yet generally unknown) ionization efficiencies compared to lower molar mass compounds. Second, the nano-DESI-HRMS analysis of toluene SOA was limited to m/z range of 100 -1000 (Hinks et al., 2017). It is possible that some SOA products with lower molar mass were present in particles but not detected, which would lead to an overestimation of T_g. Third, the chemical composition of toluene SOA are likely different between Hinks et al. (2017) and Song et al. (2016) because of the differences in the experimental conditions. Specifically, toluene SOA was formed in a Teflon chamber in Hinks et al., while Song et al. used an oxidation flow reactor to generate toluene SOA. The O:C ratios are 0.71 at low RH and 0.63 at high RH based on nano-DESI-HRMS measurements in Hinks et al. (2017), while it was 1.06 based on the aerosol mass spectrometry (AMS) measurements in Song et al. (2016).

In addition, different mass loadings may have affected viscosity. Song et al. (2016) measured viscosity at two different mass loadings (60-100 and 600-1000 μg m^{-3}) and compared their results to Bateman et al. (2015) (30-50 μg m^{-3}) and Li et al. (2015) (44-125 μg m^{-3}), observing little impact of mass loadings on viscosity. We carried out a sensitivity study of mass loadings on viscosity using a set of compounds detected by HRMS. The saturation mass concentration was predicted for each component using the molecular corridor approach (Li et al., 2016). Assuming that the mass signal intensity is proportional to the total mass concentration of the compound in the mixture, and applying the absorptive partitioning theory (Pankow, 1994), particle-phase concentrations of each compound were predicted to estimate T_g at different organic aerosol mass loading values (1-1000 μg m^{-3}). The glass transition temperature of the SOA mixture decreases as mass loading increases. Viscosity decreases up to two orders of magnitude at low RH, while at high RH they have little difference as shown in Fig. A3. Simultaneous measurements of viscosity and chemical composition with different mass loadings should be performed in future studies.

3.3 Biomass Burning Particles

To further explore the applicability of our viscosity prediction method using elemental composition as measured by HRMS, we performed similar calculations for biomass burning organic particles emitted from test facility burns of subalpine fir and lodgepole pine trees, conducted as a part of the FIREX 2016 campaign (Selimovic et al., 2017). These samples were analyzed by HRMS using two different ionization sources: electrospray ionization (ESI) and atmospheric pressure photoionization (APPI). Mass spectra shown in Fig. 8(a) and (b) indicate that a substantial number of compounds were detected by both methods (109 and 170

compounds for subalpine fur and lodgepole pine, respectively). However, pronounced differences are also observed between the ESI and APPI spectra both in terms of the identity and signal intensities of the detected compounds.

Glass transition temperatures for the assigned CH and CHO compounds were computed using Eq. (2). Nitrogen and sulfur containing compounds (CHON and CHOS) are not yet covered by Eq. (2) and were therefore excluded from the analysis. CHON and CHOS compounds comprised less than 10% of the detected ion intensity and <15% of the assigned compounds. Please note that we do not intend to provide accurate estimates of ambient biomass burning particles (as inorganic components are also not included in this analysis), but we investigate how the use of different ionization methods would lead to variations in our viscosity predictions. T_g of organic mixtures ($T_{g,org}$) were then calculated using the Gordon-Taylor approach with k_{GT} = 1, assuming that the relative concentration of each compound is proportional to its MS signal intensity. The calculated $T_{g,org}$ values for the mixtures are specified in the legend of Figure 9. For both types of mixtures, the calculated $T_{g,org}$ for the APPI MS data is lower than the value calculated based on the ESI MS data with a difference of 32 K for subalpine fir and 11 K for the lodgepole pine. Figure 9 shows the predicted viscosity as a function of RH, assuming D = 10, κ = 0.10 and k_{GT} = 2.5. The difference in $T_{g,org}$ derived from ESI and APPI results in a variation of predicted viscosity at low RH by up to five and two orders of magnitude for subalpine fir and lodgepole pine, respectively.

The difference in the calculated $T_{g,org}$ values is attributed to the chemical profile of the species detected using different ionization techniques as shown in mass spectra in Fig. 8(a) and (b). Van Krevelen diagrams in Fig. 8(c) and (d) illustrate these compositional differences between chemical species detected by ESI and APPI. ESI is more efficient at detection of polar

493 compounds (Kiontke et al., 2016), which typically have higher O:C ratios and therefore would
494 result in higher predicted values of viscosity (Koop et al., 2011; Saukko et al., 2012). APPI
495 enables the detection of nonpolar compounds with lower O:C ratios, in particular polycyclic
496 aromatic hydrocarbons (PAHs), that have low ionization efficiencies when analyzed by ESI MS
497 (Raffaelli and Saba, 2003; Itoh et al., 2006). Due to the complementary nature of these ionization
498 methods, it is most likely that the actual glass transition temperature and viscosity of each type of
499 SOA are somewhere in between the values inferred from ESI and APPI data sets: ESI MS may
500 be viewed as providing the upper limit of viscosity, while APPI MS gives the lower limit. Our
501 results indicate that the use of complementary ionization techniques may help evaluate the
502 associated uncertainty for the prediction of viscosity values based on the elemental composition
503 as measured by HRMS.
504
505 **4 Conclusions**
506 We have developed a parameterization for calculation of the glass transition temperature
507 of individual SOA compounds with molar mass up to ~1100 g mol^{-1} using the number of carbon,
508 oxygen, and hydrogen atoms. Viscosity of SOA was estimated using the T_g-scaled Arrhenius plot
509 of viscosity versus T_g/T and the Gordon-Taylor approach to account for mixtures of SOA and
510 water. The fragility parameter D was compiled for organic compounds and we found that D
511 approaches a lower limit of ~10 (+/- 1.7) as the molar mass increases. The resulting viscosity
512 estimations agree well with measured viscosity of α-pinene and isoprene SOA, validating our
513 method. Using HRMS data, glass transition temperatures of individual components and viscosity
514 of toluene SOA were predicted, also resulting in a good agreement with measurements.
515 However, we note that the predicted viscosities were slightly higher than the measured values

516 suggesting that additional considerations may need to be taken into account. For example, the
517 ionization efficiency of both low and high molar mass compounds may have a pronounced effect
518 on the relative abundance of different classes of compounds in HRMS data. The viscosity
519 prediction method was also applied to biomass burning particles, whose elemental composition
520 was measured using HRMS with two different ionization techniques. Substantial differences in
521 viscosity estimations were obtained using ESI and APPI mass spectra.

522 Figure 10 summarizes the predicted range of viscosity of α-pinene SOA, isoprene SOA,
523 toluene SOA, and biomass burning particles. Isoprene SOA has lower viscosity, reflecting lower
524 glass transition temperature due to relatively low molar mass of isoprene oxidation products. α-
525 pinene and toluene SOA have much higher viscosity with a different shape of the RH
526 dependence due to differences in glass transition temperatures and hygroscopicity. Biomass
527 burning particles have moderate viscosity between the two extreme cases. Currently, both
528 predictions and measurements are subject to large uncertainties and variations. Complementary
529 measurements of viscosity and chemical composition employing different ionization techniques
530 are desired to further constrain RH-dependent viscosity in future studies. Current T_g
531 parameterizations do not consider functionality or molecular structure explicitly and further
532 measurements of T_g and viscosity of SOA would allow us to refine the method presented in this
533 study. Nevertheless, current results offer a promising starting point and such simple
534 parameterizations are practical for predicting viscosity of particles as measured by HRMS. The
535 developed viscosity prediction method should also be useful in recent efforts of simulating the
536 distribution of SOA phase state and related properties in regional or global air quality models
537 (e.g., Maclean et al., 2017; Shiraiwa et al., 2017).
538

Appendix A: Conversion of fragility steepness index (*m*) to fragility (*D*)

Fragility steepness index (m) is defined as:

$$m = \lim_{T \to Tg} \frac{d\, log\eta}{d(T_g/T)} \tag{A1}$$

Combining Eq. (A1) with Eq. (4) gives:

$$m = \lim_{T \to Tg} \frac{d}{d(T_g/T)} \left(-5 + 0.434 \frac{T_0 D}{T - T_0} \right) \tag{A2}$$

Considering that $\eta = 10^{12}$ Pa s at $T = T_g$ (Angell, 1991), and by defining Δx = 1- T_g/T, and a combination with Eq. (5) leads to:

$$m = \lim_{\Delta x \to 0} \frac{1}{\Delta x} \left(12 - \left(-5 + 0.434 \frac{\frac{39.17\, T_g}{D + 39.17} D}{\frac{T_g}{1 - \Delta x} - \frac{39.17\, T_g}{D + 39.17}} \right) \right)$$

$$= \lim_{\Delta x \to 0} \frac{1}{\Delta x} \left(17 - 0.434 \frac{39.17 T_g D (1 - \Delta x)}{D T_g + 39.17 T_g \Delta x} \right)$$

$$= \lim_{\Delta x \to 0} \frac{(665.89 + 17D)}{(D + 39.17\Delta x)}$$

$$= \frac{665.89 + 17D}{D} \tag{A3}$$

Note that Eq. (A3) is derived assuming the high temperature limit of viscosity η_∞ is equal to 10^{-5} Pa s (Angell, 1991) in the VTF equation (Eq. 3). Similar equations for the relation between *m* and *D* were given by previous studies using different η_∞ and units (Angell et al., 1994; Angell, 2002; Bones et al., 2012) and applying those gave very similar results in our study.

Acknowledgements.

This work was funded by the National Science Foundation (AGS-1654104) and the Department of Energy (DE-SC0018349). The Purdue group and S. N. acknowledge additional support by the U.S. Department of Commerce, National Oceanic and Atmospheric Administration through

Climate Program Office's AC4 program, awards NA16OAR4310101 and NA16OAR4310102.

We thank Ulrich Pöschl and Thomas Koop for stimulating discussions.

References.

Abbatt, J. P. D., Lee, A. K. Y., and Thornton, J. A.: Quantifying trace gas uptake to tropospheric aerosol: recent advances and remaining challenges, Chem. Soc. Rev., 41, 6555-6581, 2012.

Abramson, E., Imre, D., Beranek, J., Wilson, J., and Zelenyuk, A.: Experimental determination of chemical diffusion within secondary organic aerosol particles, Physical Chemistry Chemical Physics, 15, 2983-2991, 2013.

Aiken, A. C., DeCarlo, P. F., Kroll, J. H., et al.: O/C and OM/OC Ratios of Primary, Secondary, and Ambient Organic Aerosols with High-Resolution Time-of-Flight Aerosol Mass Spectrometry, Environ. Sci. Technol., 42, 4478-4485, 2008.

Angell, C.: Relaxation in liquids, polymers and plastic crystals—strong/fragile patterns and problems, Journal of Non-Crystalline Solids, 131, 13-31, 1991.

Angell, C. A., Bressel, R. D., Green, J. L., Kanno, H., Oguni, M., and Sare, E. J.: Liquid fragility and the glass transition in water and aqueous solutions, Journal of Food Engineering, 22, 115-142, 1994.

Angell, C. A.: Formation of glasses from liquids and biopolymers, Science, 267, 1924-1935, 1995.

Angell, C. A.: Entropy and fragility in supercooling liquids, National Institute of Standards and Technology, Journal of Research, 102, 171-185, 1997.

Angell, C. A.: Liquid Fragility and the Glass Transition in Water and Aqueous Solutions, Chem. Rev., 102, 2627-2650, 2002.

Arangio, A. M., Slade, J. H., Berkemeier, T., Pöschl, U., Knopf, D. A., and Shiraiwa, M.: Multiphase Chemical Kinetics of OH Radical Uptake by Molecular Organic Markers of Biomass Burning Aerosols: Humidity and Temperature Dependence, Surface Reaction and Bulk Diffusion, J. Phys. Chem. A, 119, 4533–4544, 2015.

Bateman, A. P., Laskin, J., Laskin, A., and Nizkorodov, S. A.: Applications of High-Resolution Electrospray Ionization Mass Spectrometry to Measurements of Average Oxygen to Carbon Ratios in Secondary Organic Aerosols, Environ. Sci. Technol., 46, 8315-8324, 2012.

Bateman, A. P., Bertram, A. K., and Martin, S. T.: Hygroscopic Influence on the Semisolid-to-Liquid Transition of Secondary Organic Materials, J. Phys. Chem. A, 119, 4386-4395, 2015.

588 Bateman, A. P., Gong, Z., Liu, P., et al.: Sub-micrometre particulate matter is primarily in liquid
589 form over Amazon rainforest, Nat. Geosci., 9, 34-37, 2016.

590 Baustian, K. J., Wise, M. E., Jensen, E. J., Schill, G. P., Freedman, M. A., and Tolbert, M. A.:
591 State transformations and ice nucleation in amorphous (semi-)solid organic aerosol, Atmos.
592 Chem. Phys., 13, 5615-5628, 2013.

593 Berkemeier, T., Shiraiwa, M., Pöschl, U., and Koop, T.: Competition between water uptake and
594 ice nucleation by glassy organic aerosol particles, Atmos. Chem. Phys., 14, 12513-12531, 2014.

595 Berkemeier, T., Steimer, S., Krieger, U. K., Peter, T., Poschl, U., Ammann, M., and Shiraiwa,
596 M.: Ozone uptake on glassy, semi-solid and liquid organic matter and the role of reactive oxygen
597 intermediates in atmospheric aerosol chemistry, Phys. Chem. Chem. Phys., 18, 12662-12674,
598 2016.

599 Boehmer, R., Ngai, K. L., Angell, C. A., and Plazek, D. J.: Nonexponential relaxations in strong
600 and fragile glass formers, J. Chem. Phys., 99, 4201-4209, 1993.

601 Bones, D. L., Reid, J. P., Lienhard, D. M., and Krieger, U. K.: Comparing the mechanism of
602 water condensation and evaporation in glassy aerosol, Proc. Natl. Acad. Sci. U.S.A., 109, 11613-
603 11618, 2012.

604 Booth, A. M., Murphy, B., Riipinen, I., Percival, C. J., and Topping, D. O.: Connecting Bulk
605 Viscosity Measurements to Kinetic Limitations on Attaining Equilibrium for a Model Aerosol
606 Composition, Environ. Sci. Technol., 48, 9298-9305, 2014.

607 Cappa, C. D., and Wilson, K. R.: Evolution of organic aerosol mass spectra upon heating:
608 implications for OA phase and partitioning behavior, Atmos. Chem. Phys., 11, 1895-1911, 2011.

609 Cappa, C. D., and Wilson, K. R.: Multi-generation gas-phase oxidation, equilibrium partitioning,
610 and the formation and evolution of secondary organic aerosol, Atmos. Chem. Phys., 12, 9505-
611 9528, 2012.

612 Chen, Q., Liu, Y., Donahue, N. M., Shilling, J. E., and Martin, S. T.: Particle-Phase Chemistry of
613 Secondary Organic Material: Modeled Compared to Measured O:C and H:C Elemental Ratios
614 Provide Constraints, Environ. Sci. Technol., 45, 4763–4770, 2011.

615 Davies, J. F., and Wilson, K. R.: Nanoscale interfacial gradients formed by the reactive uptake of
616 OH radicals onto viscous aerosol surfaces, Chem. Sci., 6, 7020-7027, 2015.

617 Dette, H. P., Qi, M., Schröder, D. C., Godt, A., and Koop, T.: Glass-forming properties of 3-
618 Methylbutane-1,2,3-tricarboxylic acid and its mixtures with water and pinonic acid, J. Phys.
619 Chem. A, 118, 7024-7033, 2014.

620 Dette, H. P., and Koop, T.: Glass Formation Processes in Mixed Inorganic/Organic Aerosol
621 Particles, J. Phys. Chem. A, 119, 4552-4561, 2015.

622 Donahue, N. M., Robinson, A. L., Stanier, C. O., and Pandis, S. N.: Coupled partitioning,
623 dilution, and chemical aging of semivolatile organics, Environ. Sci. Technol., 40, 2635-2643,
624 2006.

625 Donahue, N. M., Epstein, S. A., Pandis, S. N., and Robinson, A. L.: A two-dimensional volatility
626 basis set: 1. organic-aerosol mixing thermodynamics, Atmos. Chem. Phys., 11, 3303-3318, 2011.

627 Fox Jr, T. G., and Flory, P. J.: Second‐order transition temperatures and related properties of
628 polystyrene. I. Influence of molecular weight, J. Appl. Phys., 21, 581-591, 1950.

629 Gao, S., Ng, N. L., Keywood, M., et al.: Particle phase acidity and oligomer formation in
630 secondary organic aerosol, Environ. Sci. Technol., 38, 6582-6589, 2004.

631 Goldstein, A. H., and Galbally, I. E.: Known and unexplored organic constituents in the earth's
632 atmosphere, Environ. Sci. Technol., 41, 1514-1521, 2007.

633 Gorkowski, K., Donahue, N. M., and Sullivan, R. C.: Emulsified and Liquid–Liquid Phase-
634 Separated States of α-Pinene Secondary Organic Aerosol Determined Using Aerosol Optical
635 Tweezers, Environ. Sci. Technol., 51, 12154-12163, 2017.

636 Grayson, J. W., Zhang, Y., Mutzel, A., Renbaum-Wolff, L., Böge, O., Kamal, S., Herrmann, H.,
637 Martin, S. T., and Bertram, A. K.: Effect of varying experimental conditions on the viscosity of
638 α-pinene derived secondary organic material, Atmos. Chem. Phys., 16, 6027-6040, 2016.

639 Grayson, J. W., Evoy, E., Song, M., et al.: The effect of hydroxyl functional groups and molar
640 mass on the viscosity of non-crystalline organic and organic–water particles, Atmos. Chem.
641 Phys., 17, 8509-8524, 2017.

642 Gunthe, S. S., King, S. M., Rose, D., et al.: Cloud condensation nuclei in pristine tropical
643 rainforest air of Amazonia: size-resolved measurements and modeling of atmospheric aerosol
644 composition and CCN activity, Atmos. Chem. Phys., 9, 7551-7575, 2009.

645 Hancock, B. C., and Zografi, G.: The relationship between the glass transition temperature and
646 the water content of amorphous pharmaceutical solids, Pharm. Res., 11, 471-477, 1994.

647 Hildebrandt Ruiz, L., Paciga, A. L., Cerully, K. M., Nenes, A., Donahue, N. M., and Pandis, S.
648 N.: Formation and aging of secondary organic aerosol from toluene: changes in chemical
649 composition, volatility, and hygroscopicity, Atmos. Chem. Phys., 15, 8301-8313, 2015.

650 Hinks, M. L., Brady, M. V., Lignell, H., et al.: Effect of viscosity on photodegradation rates in
651 complex secondary organic aerosol materials, Phys. Chem. Chem. Phys., 18, 8785-8793, 2016.

652 Hinks, M. L., Montoya-Aguilera, J., Ellison, L., Lin, P., Laskin, A., Laskin, J., Shiraiwa, M.,
653 Dabdub, D., and Nizkorodov, S. A.: Effect of Relative Humidity on the Composition of
654 Secondary Organic Aerosol from Oxidation of Toluene, Atmos. Chem. Phys. Discuss., 2017, 1-
655 16, 2017.

Hinks, M. L., Montoya-Aguilera, J., Ellison, L., Lin, P., Laskin, A., Laskin, J., Shiraiwa, M., Dabdub, D., and Nizkorodov, S. A.: Effect of relative humidity on the composition of secondary organic aerosol from the oxidation of toluene, Atmos. Chem. Phys., 18, 1643-1652, 2018.

Hosny, N. A., Fitzgerald, C., Vysniauskas, A., et al.: Direct imaging of changes in aerosol particle viscosity upon hydration and chemical aging, Chem. Sci., 7, 1357-1367, 2016.

Huang, D., and McKenna, G. B.: New insights into the fragility dilemma in liquids, J. Chem. Phys., 114, 5621-5630, 2001.

Huang, W., Saathoff, H., Pajunoja, A., Shen, X., Naumann, K. H., Wagner, R., Virtanen, A., Leisner, T., and Mohr, C.: α-Pinene secondary organic aerosol at low temperature: chemical composition and implications for particle viscosity, Atmos. Chem. Phys., 18, 2883-2898, 2018.

Ignatius, K., Kristensen, T. B., Järvinen, E., et al.: Heterogeneous ice nucleation of viscous secondary organic aerosol produced from ozonolysis of α-pinene, Atmos. Chem. Phys., 16, 6495-6509, 2016.

Itoh, N., Aoyagi, Y., and Yarita, T.: Optimization of the dopant for the trace determination of polycyclic aromatic hydrocarbons by liquid chromatography/dopant-assisted atmospheric-pressure photoionization/mass spectrometry, J. Chromatogr. A, 1131, 285-288, 2006.

Jain, S., and Petrucci, G. A.: A New Method to Measure Aerosol Particle Bounce Using a Cascade Electrical Low Pressure Impactor, Aerosol Sci. Technol., 49, 390-399, 2015.

Jathar, S. H., Cappa, C. D., Wexler, A. S., Seinfeld, J. H., and Kleeman, M. J.: Multi-generational oxidation model to simulate secondary organic aerosol in a 3-D air quality model, Geosci. Model Dev., 8, 2553-2567, 2015.

Jimenez, J. L., Canagaratna, M. R., Donahue, N. M., et al.: Evolution of organic aerosols in the atmosphere, Science, 326, 1525-1529, 2009.

Kidd, C., Perraud, V., Wingen, L. M., and Finlayson-Pitts, B. J.: Integrating phase and composition of secondary organic aerosol from the ozonolysis of alpha-pinene, Proc. Natl. Acad. Sci. U.S.A., 111, 7552-7557, 2014.

Kiontke, A., Oliveira-Birkmeier, A., Opitz, A., and Birkemeyer, C.: Electrospray ionization efficiency is dependent on different molecular descriptors with respect to solvent ph and instrumental configuration, PLoS One, 11, e0167502/0167501-e0167502/0167516, 2016.

Knopf, D. A., Alpert, P. A., and Wang, B.: The Role of Organic Aerosol in Atmospheric Ice Nucleation: A Review, ACS Earth and Space Chemistry, 2018.

Koop, T., Bookhold, J., Shiraiwa, M., and Pöschl, U.: Glass transition and phase state of organic compounds: dependency on molecular properties and implications for secondary organic aerosols in the atmosphere, Phys. Chem. Chem. Phys., 13, 19238-19255, 2011.

690 Kuwata, M., and Martin, S. T.: Phase of atmospheric secondary organic material affects its
691 reactivity, Proc. Natl. Acad. Sci. U.S.A., 109, 17354-17359, 2012.

692 Kuwata, M., Zorn, S. R., and Martin, S. T.: Using elemental ratios to predict the density of
693 organic material composed of carbon, hydrogen, and oxygen, Environ. Sci. Technol., 46, 787-
694 794, 2012.

695 Lambe, A. T., Ahern, A. T., Williams, L. R., et al.: Characterization of aerosol photooxidation
696 flow reactors: heterogeneous oxidation, secondary organic aerosol formation and cloud
697 condensation nuclei activity measurements, Atmos. Meas. Tech., 4, 445-461, 2011a.

698 Lambe, A. T., Onasch, T. B., Massoli, P., et al.: Laboratory studies of the chemical composition
699 and cloud condensation nuclei (CCN) activity of secondary organic aerosol (SOA) and oxidized
700 primary organic aerosol (OPOA), Atmos. Chem. Phys., 11, 8913-8928, 2011b.

701 Li, Y., Pöschl, U., and Shiraiwa, M.: Molecular corridors and parameterizations of volatility in
702 the chemical evolution of organic aerosols, Atmos. Chem. Phys., 16, 3327-3344, 2016.

703 Li, Y. J., Liu, P., Gong, Z., Wang, Y., Bateman, A. P., Bergoend, C., Bertram, A. K., and Martin,
704 S. T.: Chemical Reactivity and Liquid/Nonliquid States of Secondary Organic Material, Environ.
705 Sci. Technol., 49, 13264-13274, 2015.

706 Lienhard, D. M., Huisman, A. J., Krieger, U. K., et al.: Viscous organic aerosol particles in the
707 upper troposphere: diffusivity-controlled water uptake and ice nucleation?, Atmos. Chem. Phys.,
708 15, 13599-13613, 2015.

709 Lignell, H., Hinks, M. L., and Nizkorodov, S. A.: Exploring matrix effects on photochemistry of
710 organic aerosols, Proc. Natl. Acad. Sci. U.S.A., 111, 13780-13785, 2014.

711 Liu, P., Li, Y. J., Wang, Y., Gilles, M. K., Zaveri, R. A., Bertram, A. K., and Martin, S. T.:
712 Lability of secondary organic particulate matter, Proc. Natl. Acad. Sci. U.S.A., 113, 12643-
713 12648, 2016.

714 Liu, P., Li, Y. J., Wang, Y., Bateman, A. P., Zhang, Y., Gong, Z., Bertram, A. K., and Martin, S.
715 T.: Highly Viscous States Affect the Browning of Atmospheric Organic Particulate Matter, ACS
716 Central Science, 4, 207-215, 2018.

717 Loza, C. L., Coggon, M. M., Nguyen, T. B., Zuend, A., Flagan, R. C., and Seinfeld, J. H.: On the
718 mixing and evaporation of secondary organic aerosol components, Environ. Sci. Technol., 47,
719 6173-6180, 2013.

720 Maclean, A. M., Butenhoff, C. L., Grayson, J. W., Barsanti, K., Jimenez, J. L., and Bertram, A.
721 K.: Mixing times of organic molecules within secondary organic aerosol particles: a global
722 planetary boundary layer perspective, Atmos. Chem. Phys., 17, 13037-13048, 2017.

723 Mai, H., Shiraiwa, M., Flagan, R. C., and Seinfeld, J. H.: Under What Conditions Can
724 Equilibrium Gas–Particle Partitioning Be Expected to Hold in the Atmosphere?, Environ. Sci.
725 Technol., 49, 11485-11491, 2015.

Marshall, F. H., Miles, R. E. H., Song, Y.-C., Ohm, P. B., Power, R. M., Reid, J. P., and Dutcher, C. S.: Diffusion and reactivity in ultraviscous aerosol and the correlation with particle viscosity, Chem. Sci., 7, 1298-1308, 2016.

Matsushima, S., Takano, A., Takahashi, Y., and Matsushita, Y.: Precise synthesis of a series of poly(4-n-alkylstyrene)s and their glass transition temperatures, Journal of Polymer Science Part B: Polymer Physics, 55, 757-763, 2017.

Metatla, N., and Soldera, A.: The Vogel− Fulcher− Tamman Equation Investigated by Atomistic Simulation with Regard to the Adam− Gibbs Model, Macromolecules, 40, 9680-9685, 2007.

Mikhailov, E., Vlasenko, S., Martin, S. T., Koop, T., and Pöschl, U.: Amorphous and crystalline aerosol particles interacting with water vapor: conceptual framework and experimental evidence for restructuring, phase transitions and kinetic limitations, Atmos. Chem. Phys., 9, 9491-9522, 2009.

Montserrat, S., and Colomer, P.: The effect of the molecular weight on the glass transition temperature in amorphous poly(ethylene terephthalate), Polymer Bulletin, 12, 173-180, 1984.

Murray, B. J., Wilson, T. W., Dobbie, S., et al.: Heterogeneous nucleation of ice particles on glassy aerosols under cirrus conditions, Nat. Geosci., 3, 233-237, 2010.

Nakanishi, M., and Nozaki, R.: Systematic study of the glass transition in polyhydric alcohols, Physical Review E, 83, 051503, 2011.

Nguyen, T. B., Nizkorodov, S. A., Laskin, A., and Laskin, J.: An approach toward quantification of organic compounds in complex environmental samples using high-resolution electrospray ionization mass spectrometry, Anal. Methods, 5, 72-80, 2013.

Nizkorodov, S. A., Laskin, J., and Laskin, A.: Molecular chemistry of organic aerosols through the application of high resolution mass spectrometry, Phys. Chem. Chem. Phys., 13, 3612-3629, 2011.

Nozière, B., Kalberer, M., Claeys, M., et al.: The Molecular Identification of Organic Compounds in the Atmosphere: State of the Art and Challenges, Chem. Rev., 115, 3919–3983, 2015.

O'Connell, P. A., and McKenna, G. B.: Arrhenius-type temperature dependence of the segmental relaxation below T g, J. Chem. Phys., 110, 11054-11060, 1999.

Onder, K., Peters, R. H., and Spark, L. C.: Melting and transition phenomena in some polyester-urethanes, Polymer, 13, 133-139, 1972.

Pajunoja, A., Malila, J., Hao, L., Joutsensaari, J., Lehtinen, K. E. J., and Virtanen, A.: Estimating the viscosity range of SOA particles based on their coalescence time, Aerosol Sci. Technol., 48, i-iv, 2014.

760 Pajunoja, A., Lambe, A. T., Hakala, J., et al.: Adsorptive uptake of water by semisolid secondary
761 organic aerosols, Geophys. Res. Lett., 42, 3063-3068, 2015.

762 Papadopoulos, P., Floudas, G., Chi, C., and Wegner, G.: Molecular dynamics of oligofluorenes:
763 A dielectric spectroscopy investigation, J. Chem. Phys., 120, 2368-2374, 2004.

764 Perraud, V., Bruns, E. A., Ezell, M. J., et al.: Nonequilibrium atmospheric secondary organic
765 aerosol formation and growth, Proc. Natl. Acad. Sci. U.S.A., 109, 2836-2841, 2012.

766 Petters, M. D., and Kreidenweis, S. M.: A single parameter representation of hygroscopic growth
767 and cloud condensation nucleus activity, Atmos. Chem. Phys., 7, 1961-1971, 2007.

768 Petters, S. S., Pagonis, D., Claflin, M. S., Levin, E. J. T., Petters, M. D., Ziemann, P. J., and
769 Kreidenweis, S. M.: Hygroscopicity of Organic Compounds as a Function of Carbon Chain
770 Length and Carboxyl, Hydroperoxy, and Carbonyl Functional Groups, J. Phys. Chem. A, 121,
771 5164-5174, 2017.

772 Polymer handbook, t. e.: J. Brandrup (Editor), Edmund H. Immergut (Editor), E. A. Grulke
773 (Editor), John Wiley & Sons, Inc., ISBN 0-471-16628-6, 1999.

774 Pratap, V., Chen, Y., Yao, G., and Nakao, S.: Temperature effects on multiphase reactions of
775 organic molecular markers: A modeling study, Atmos. Environ., 179, 40-48, 2018.

776 Price, H. C., Murray, B. J., Mattsson, J., O'Sullivan, D., Wilson, T. W., Baustian, K. J., and
777 Benning, L. G.: Quantifying water diffusion in high-viscosity and glassy aqueous solutions using
778 a Raman isotope tracer method, Atmos. Chem. Phys., 14, 3817-3830, 2014.

779 Putman, A. L., Offenberg, J. H., Fisseha, R., Kundu, S., Rahn, T. A., and Mazzoleni, L. R.:
780 Ultrahigh-resolution FT-ICR mass spectrometry characterization of α-pinene ozonolysis SOA,
781 Atmos. Environ., 46, 164-172, 2012.

782 Raffaelli, A., and Saba, A.: Atmospheric pressure photoionization mass spectrometry, Mass
783 Spectrom. Rev., 22, 318-331, 2003.

784 Reid, J. P., Bertram, A. K., Topping, D. O., Laskin, A., Martin, S. T., Petters, M. D., Pope, F. D.,
785 and Rovelli, G.: The viscosity of atmospherically relevant organic particles, Nat. Commun., 9,
786 956, 2018.

787 Renbaum-Wolff, L., Grayson, J. W., Bateman, A. P., Kuwata, K., Sellier, M., Murray, B. J.,
788 Schilling, J. E., Martin, S. T., and Bertram, A. K.: Viscosity of α-pinene secondary organic
789 material and implications for particle growth and reactivity, Proc. Natl. Acad. Sci. U.S.A., 110,
790 8014-8019, 2013.

791 Roach, P. J., Laskin, J., and Laskin, A.: Nanospray desorption electrospray ionization: an
792 ambient method for liquid-extraction surface sampling in mass spectrometry, Analyst
793 (Cambridge, U. K.), 135, 2233-2236, 2010a.

794 Roach, P. J., Laskin, J., and Laskin, A.: Molecular Characterization of Organic Aerosols Using
795 Nanospray-Desorption/Electrospray Ionization-Mass Spectrometry, Anal. Chem. (Washington,
796 DC, U. S.), 82, 7979-7986, 2010b.

797 Roldin, P., Eriksson, A. C., Nordin, E. Z., et al.: Modelling non-equilibrium secondary organic
798 aerosol formation and evaporation with the aerosol dynamics, gas- and particle-phase chemistry
799 kinetic multilayer model ADCHAM, Atmos. Chem. Phys., 14, 7953-7993, 2014.

800 Roos, Y.: Melting and glass transitions of low molecular weight carbohydrates, Carbohydr. Res.,
801 238, 39-48, 1993.

802 Rothfuss, N. E., and Petters, M. D.: Influence of Functional Groups on the Viscosity of Organic
803 Aerosol, Environ. Sci. Technol., 51, 271-279, 2017.

804 Sastri, S. R. S., and Rao, K. K.: A new group contribution method for predicting viscosity of
805 organic liquids, The Chemical Engineering Journal, 50, 9-25, 1992.

806 Saukko, E., Lambe, A. T., Massoli, P., et al.: Humidity-dependent phase state of SOA particles
807 from biogenic and anthropogenic precursors, Atmos. Chem. Phys., 12, 7517-7529, 2012.

808 Schill, G. P., and Tolbert, M. A.: Heterogeneous ice nucleation on phase-separated organic-
809 sulfate particles: effect of liquid vs. glassy coatings, Atmos. Chem. Phys., 13, 4681-4695, 2013.

810 Schill, G. P., De Haan, D. O., and Tolbert, M. A.: Heterogeneous Ice Nucleation on Simulated
811 Secondary Organic Aerosol, Environ. Sci. Technol., 48, 1675-1682, 2014.

812 Selimovic, V., Yokelson, R. J., Warneke, C., Roberts, J. M., de Gouw, J., Reardon, J., and
813 Griffith, D. W. T.: Aerosol optical properties and trace gas emissions by PAX and OP-FTIR for
814 laboratory-simulated western US wildfires during FIREX, Atmos. Chem. Phys. Discuss., 2017,
815 1-34, 2017.

816 Shiraiwa, M., Ammann, M., Koop, T., and Pöschl, U.: Gas uptake and chemical aging of
817 semisolid organic aerosol particles, Proc. Natl. Acad. Sci. U.S.A., 108, 11003-11008, 2011.

818 Shiraiwa, M., and Seinfeld, J. H.: Equilibration timescale of atmospheric secondary organic
819 aerosol partitioning, Geophys. Res. Lett., 39, L24801, 2012.

820 Shiraiwa, M., Yee, L. D., Schilling, K. A., Loza, C. L., Craven, J. S., Zuend, A., Ziemann, P. J.,
821 and Seinfeld, J. H.: Size distribution dynamics reveal particle-phase chemistry in organic aerosol
822 formation, Proc. Natl. Acad. Sci. U.S.A., 110, 11746-11750, 2013.

823 Shiraiwa, M., Berkemeier, T., Schilling-Fahnestock, K. A., Seinfeld, J. H., and Pöschl, U.:
824 Molecular corridors and kinetic regimes in the multiphase chemical evolution of secondary
825 organic aerosol, Atmos. Chem. Phys., 14, 8323-8341, 2014.

826 Shiraiwa, M., Li, Y., Tsimpidi, A. P., Karydis, V. A., Berkemeier, T., Pandis, S. N., Lelieveld, J.,
827 Koop, T., and Pöschl, U.: Global distribution of particle phase state in atmospheric secondary
828 organic aerosols, Nat. Commun., 8, 15002, 2017.

829 Shrivastava, M., Cappa, C. D., Fan, J., et al.: Recent advances in understanding secondary
830 organic aerosol: Implications for global climate forcing, Rev. Geophys., 55, 509-559, 2017.

831 Slade, J. H., and Knopf, D. A.: Multiphase OH Oxidation Kinetics of Organic Aerosol: The Role
832 of Particle Phase State and Relative Humidity, Geophys. Res. Lett., 2014GL060582, 2014.

833 Song, M., Liu, P. F., Hanna, S. J., Li, Y. J., Martin, S. T., and Bertram, A. K.: Relative humidity-
834 dependent viscosities of isoprene-derived secondary organic material and atmospheric
835 implications for isoprene-dominant forests, Atmos. Chem. Phys., 15, 5145-5159, 2015.

836 Song, M., Liu, P. F., Hanna, S. J., Zaveri, R. A., Potter, K., You, Y., Martin, S. T., and Bertram,
837 A. K.: Relative humidity-dependent viscosity of secondary organic material from toluene photo-
838 oxidation and possible implications for organic particulate matter over megacities, Atmos. Chem.
839 Phys., 16, 8817-8830, 2016a.

840 Song, Y. C., Haddrell, A. E., Bzdek, B. R., Reid, J. P., Bannan, T., Topping, D. O., Percival, C.,
841 and Cai, C.: Measurements and Predictions of Binary Component Aerosol Particle Viscosity, J.
842 Phys. Chem. A, 120, 8123-8137, 2016b.

843 Tolocka, M. P., Jang, M., Ginter, J. M., Cox, F. J., Kamens, R. M., and Johnston, M. V.:
844 Formation of oligomers in secondary organic aerosol, Environ. Sci. Technol., 38, 1428-1434,
845 2004.

846 US-EPA: Estimation programs interface suite for microsoft windows, 2012.

847 Vaden, T. D., Imre, D., Beranek, J., Shrivastava, M., and Zelenyuk, A.: Evaporation kinetics and
848 phase of laboratory and ambient secondary organic aerosol, Proc. Natl. Acad. Sci. U.S.A., 108,
849 2190-2195, 2011.

850 van der Sman, R. G. M.: Predictions of Glass Transition Temperature for Hydrogen Bonding
851 Biomaterials, J. Phys. Chem. B, 117, 16303-16313, 2013.

852 Virtanen, A., Joutsensaari, J., Koop, T., et al.: An amorphous solid state of biogenic secondary
853 organic aerosol particles, Nature, 467, 824-827, 2010.

854 Wang, B., O'Brien, R. E., Kelly, S. T., Shilling, J. E., Moffet, R. C., Gilles, M. K., and Laskin,
855 A.: Reactivity of Liquid and Semisolid Secondary Organic Carbon with Chloride and Nitrate in
856 Atmospheric Aerosols, J. Phys. Chem. A, 119, 4498-4508, 2015.

857 Wang, B. B., Lambe, A. T., Massoli, P., Onasch, T. B., Davidovits, P., Worsnop, D. R., and
858 Knopf, D. A.: The deposition ice nucleation and immersion freezing potential of amorphous
859 secondary organic aerosol: Pathways for ice and mixed-phase cloud formation, J. Geophys. Res.-
860 Atmos., 117, D16209, 2012a.

861 Wang, B. B., Laskin, A., Roedel, T., Gilles, M. K., Moffet, R. C., Tivanski, A. V., and Knopf, D.
862 A.: Heterogeneous ice nucleation and water uptake by field-collected atmospheric particles
863 below 273 K, J. Geophys. Res.-Atmos., 117, D00v19, 2012b.

White, R. P., and Lipson, J. E. G.: Polymer free volume and its connection to the glass transition, Macromolecules, 49, 3987-4007, 2016.

Williams, M. L., Landel, R. F., and Ferry, J. D.: The temperature dependence of relaxation mechanisms in amorphous polymers and other glass-forming liquids, J. Am. Chem. Soc., 77, 3701-3707, 1955.

Ye, Q., Robinson, E. S., Ding, X., Ye, P., Sullivan, R. C., and Donahue, N. M.: Mixing of secondary organic aerosols versus relative humidity, Proc. Natl. Acad. Sci. U.S.A., 113, 12649-12654, 2016.

Ye, Q., Upshur, M. A., Robinson, E. S., Geiger, F. M., Sullivan, R. C., Thomson, R. J., and Donahue, N. M.: Following Particle-Particle Mixing in Atmospheric Secondary Organic Aerosols by Using Isotopically Labeled Terpenes, Chem, 4, 318-333, 2018.

Yli-Juuti, T., Pajunoja, A., Tikkanen, O.-P., et al.: Factors controlling the evaporation of secondary organic aerosol from α-pinene ozonolysis, Geophys. Res. Lett., 44, 2562-2570, 2017.

You, Y., Smith, M. L., Song, M., Martin, S. T., and Bertram, A. K.: Liquid-liquid phase separation in atmospherically relevant particles consisting of organic species and inorganic salts, Int. Rev. Phys. Chem., 33, 43-77, 2014.

Zaveri, R. A., Easter, R. C., Shilling, J. E., and Seinfeld, J. H.: Modeling kinetic partitioning of secondary organic aerosol and size distribution dynamics: representing effects of volatility, phase state, and particle-phase reaction, Atmos. Chem. Phys., 14, 5153-5181, 2014.

Zaveri, R. A., Shilling, J. E., Zelenyuk, A., et al.: Growth Kinetics and Size Distribution Dynamics of Viscous Secondary Organic Aerosol, Environ. Sci. Technol., 52, 1191-1199, 2018.

Zhang, Y., Sanchez, M. S., Douet, C., et al.: Changing shapes and implied viscosities of suspended submicron particles, Atmos. Chem. Phys., 15, 7819-7829, 2015.

Zhang, Y., Chen, Y., Lambe, A. T., et al.: Effect of the Aerosol-Phase State on Secondary Organic Aerosol Formation from the Reactive Uptake of Isoprene-Derived Epoxydiols (IEPOX), Environ. Sci. Technol. Lett., 2018.

Zhou, S., Shiraiwa, M., McWhinney, R., Pöschl, U., and Abbatt, J. P. D.: Kinetic limitations in gas-particle reactions arising from slow diffusion in secondary organic aerosol, Faraday Discuss., 165, 391-406, 2013.

Zobrist, B., Marcolli, C., Pedernera, D. A., and Koop, T.: Do atmospheric aerosols form glasses?, Atmos. Chem. Phys., 8, 5221-5244, 2008.

Zobrist, B., Soonsin, V., Luo, B. P., Krieger, U. K., Marcolli, C., Peter, T., and Koop, T.: Ultra-slow water diffusion in aqueous sucrose glasses, Phys. Chem. Chem. Phys., 13, 3514-3526, 2011.

Table 1. Composition classes and the n_C^0 and b values (K) for glass transition temperature parameterizations obtained by least-squares optimization using the measurements compiled in Koop et al., (2011), Dette et al., (2014) and Rothfuss and Petters (2017).

Classes	n_C^0	b_C	b_H	b_{CH}	b_O	b_{CO}
CH	1.96 (±1.81)	61.99 (±53.65)	–113.33 (±44.47)	28.74 (±20.86)		
CHO	12.13 (±2.66)	10.95 (±13.60)	–41.82 (±14.78)	21.61 (±5.30)	118.96 (±9.72)	–24.38 (±4.21)

Table 2. Glass transition temperatures calculated using Eq. (1) and (2) for toluene SOA mixtures at low relative humidity (low RH < 2%) and high relative humidity (high RH = 75%) conditions.

$T_{g,org}$ (K)	low RH	high RH
Equation (1)*	299	295
Equation (2)	313	303

* Compounds with M > 450 g mol^{-1} were excluded from the analysis.

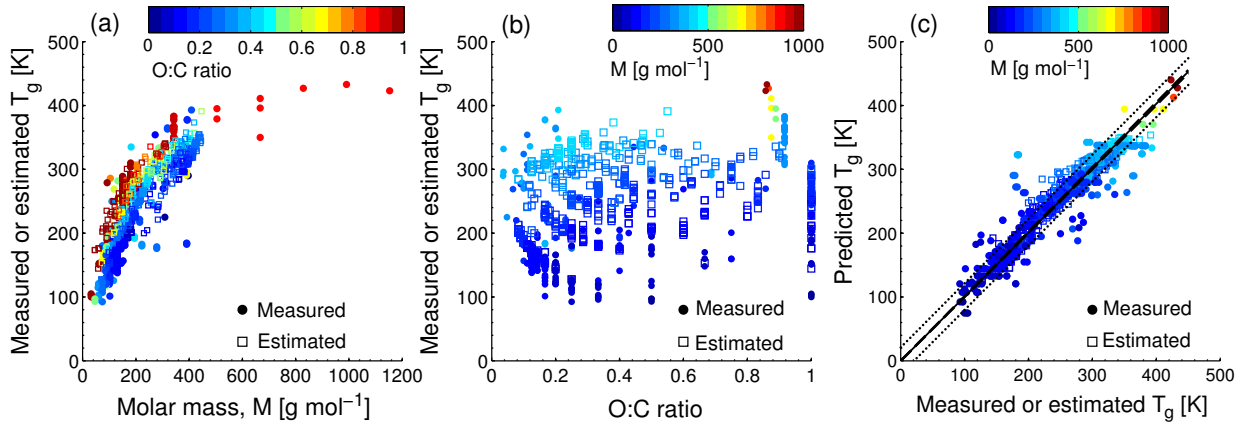

Figure 1. Characteristic relationships between molecular properties and the glass transition temperature (T_g) of organic compounds. (a) T_g of organic compounds as measured (circles) and estimated with the Boyer-Kauzmann rule (squares) plotted against molar mass. The markers are color-coded by atomic O:C ratio. (b) Measured (circles) and estimated (squares) T_g of organic compounds plotted against O:C ratio. The markers are color-coded by molar mass. (c) Predicted T_g for CHO compounds using a parameterization (Eq. 2) developed in this study compared to measured (circles) and estimated T_g by the Boyer-Kauzmann rule (squares). The solid line shows 1:1 line and the dashed and dotted lines show 68% confidence and prediction bands, respectively.

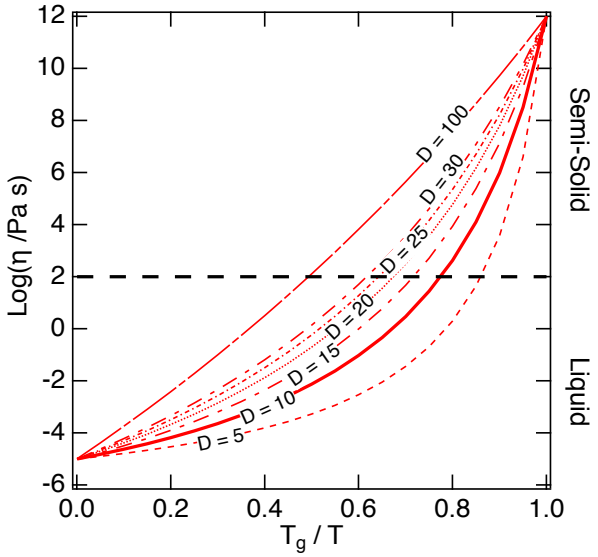

Figure 2. The Angell plot of viscosity (η) vs. T_g/T. The lines represent different fragility parameter (D) values in the range of 5 - 100, with D = 10 (the solid line) used as a base case for this study. A large fragility parameter value is associated with a strong glass former, while fragile materials are associated with lower values. The black dashed line at viscosity of 10^2 Pa s indicates the approximate threshold between liquid and semi-solid states.

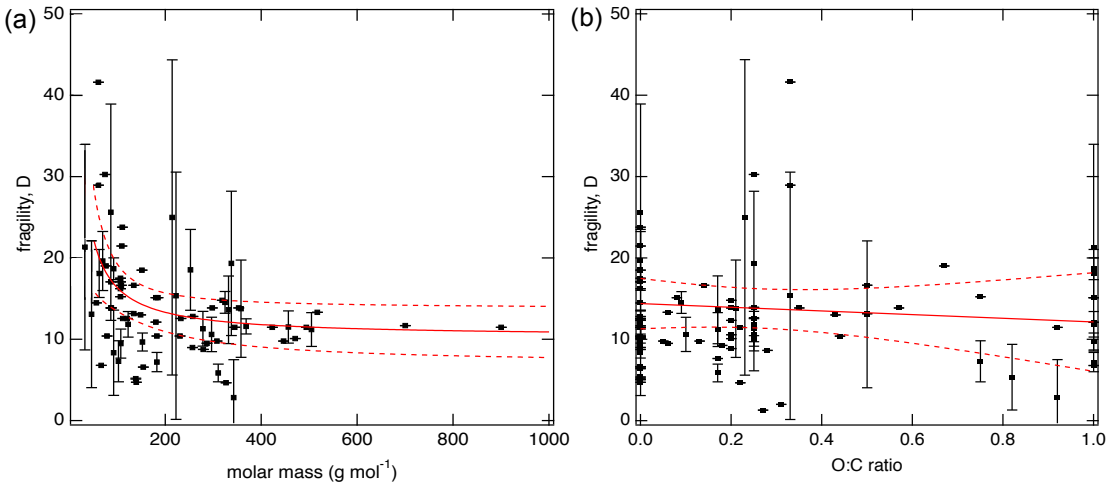

Figure 3. Fragility parameter of organic compounds (D) plotted against (a) molar mass and (b) atomic O:C ratio. Error bars are standard deviations. The solid red lines represent the fitted curves with fitted equations for (a) $D = 602.6/M + 10.3$ and (b) $D = 14.4 - 2.3(\mathrm{O{:}C})$ respectively. Dashed red lines indicate the 95% confidence band.

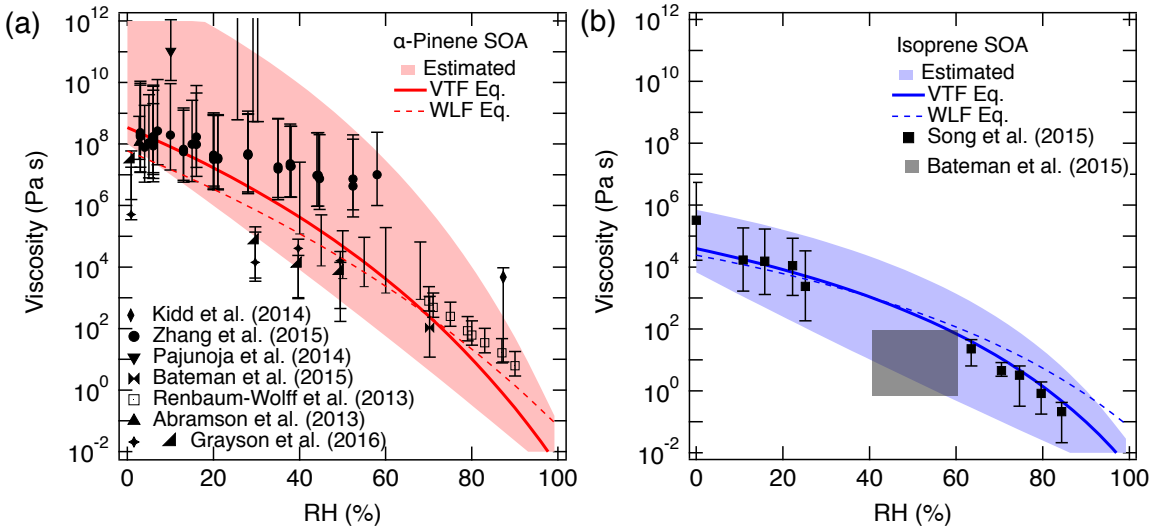

Figure 4. Comparison of measured and predicted viscosity of (a) α-pinene SOA and (b) isoprene SOA at 295 K as a function of RH. The solid lines represent base simulations with the VTF equation, while the dotted line represents viscosity predicted using the WLF equation [parameters: glass transition temperature of dry SOA ($T_{g,org}$), fragility (D), hygroscopicity (κ) and Gordon-Taylor constant (k_{GT})]: (a) 278.5 K, 0.1, 10 and 2.5; (b) 255 K, 0.1, 10 and 2.5. The shaded regions were determined by varying these parameters (a) upper (lower) limit: $T_{g,org}$ = 300 K (278.5 K), κ = 0.1 (0.1), D = 20 (10), k_{GT} = 2.5 (2.0); (b) upper (lower limit): $T_{g,org}$ = 255 K (255 K), κ = 0.10 (0.15), D = 15 (8), k_{GT} = 2.5 (4.0). Panel (a): Renbaum-Wolff et al. (2013) data represents viscosity for water-soluble portion of SOA; Grayson et al. (2016) data in the panel (a) represents two different mass loadings (121 μg m^{-3}; 520 μg m^{-3}). Panel (b): The gray box in panel (b) represents estimated viscosity based on bounce measurements of Bateman et al. (2015).

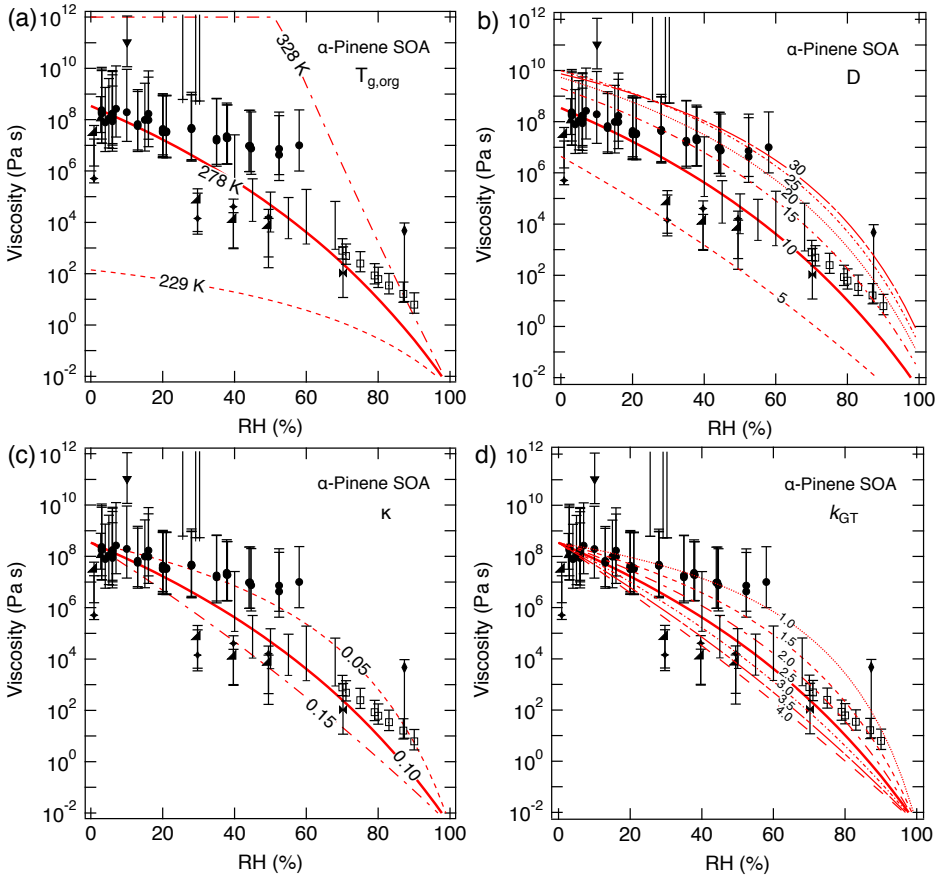

Figure 5. Sensitivity calculations for viscosity of α-pinene SOA at 295 K as a function of RH by varying: (a) glass transition temperature of dry SOA ($T_{g,org}$), (b) fragility (D), (c) hygroscopicity (κ), and (d) Gordon-Taylor constant (k_{GT}).

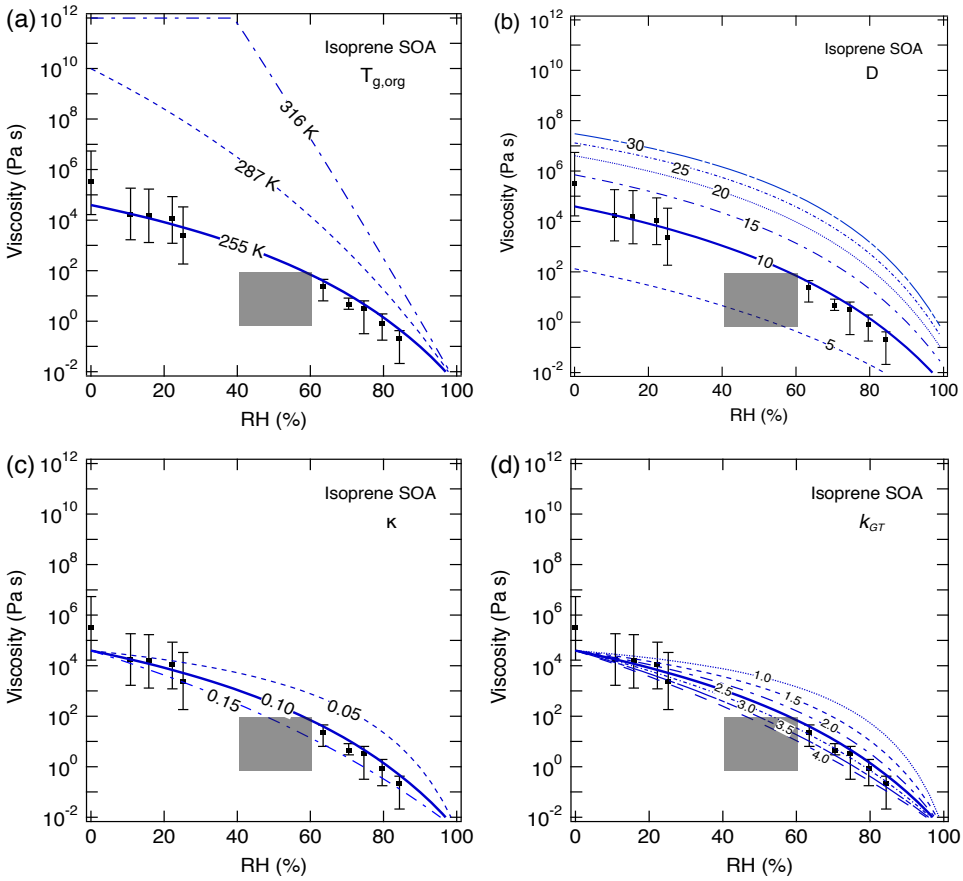

952
953
954 **Figure 6.** Sensitivity calculations for viscosity of isoprene SOA at 295 K as a function of RH by
955 varying: (a) glass transition temperature of dry SOA ($T_{g,org}$), (b) fragility (D), (c) hygroscopicity
956 (κ), and (d) Gordon-Taylor constant (k_{GT}). Data points are measured viscosity by Song et al.
957 (2015) and the gray box represents estimated viscosity based on bounce measurements of
958 Bateman et al. (2015).
959

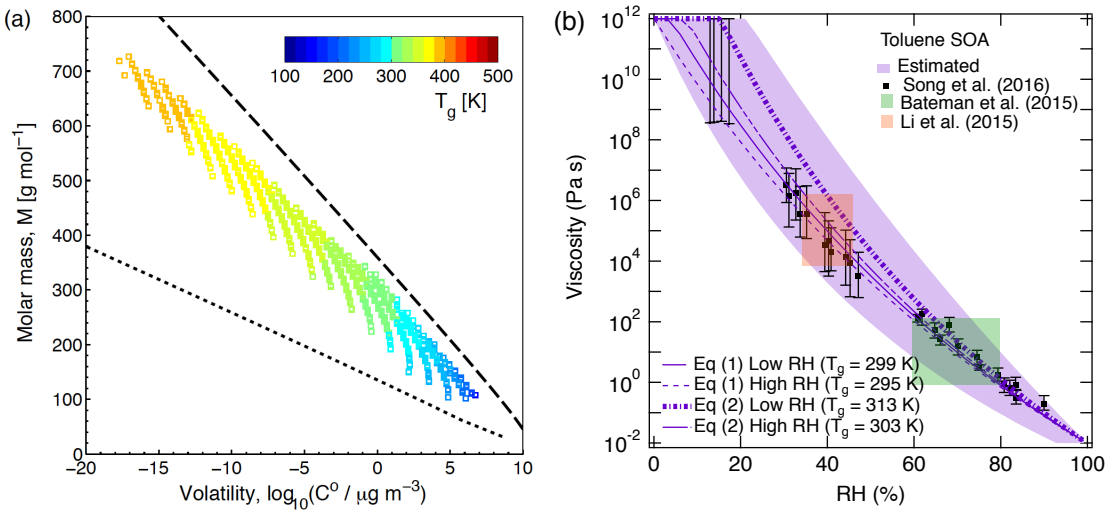

Figure 7. (a) Molecular corridor of molar mass plotted against volatility of toluene SOA formed under dry conditions (Hinks et al., 2017) color-coded by glass transition temperature (T_g) estimated using Eq. (2). The upper dashed line indicates the low O:C bound of the molecular corridor (linear alkanes C_nH_{2n+2} with O:C = 0), and the lower dotted line indicates the high O:C bound (sugar alcohols $C_nH_{2n+2}O_n$ with O:C = 1). (b) Comparison of measured (markers) and modeled (lines) viscosity of toluene SOA at 295 K as a function of RH. Viscosities were calculated using fragility (D) of 13, the hygroscopicity (κ) of 0.25 and the Gordon-Taylor constant (k_{GT}) of 3.0 with different glass transition temperatures of dry SOA ($T_{g,org}$) as estimated using Eq. (1) or (2) under low and high RH conditions. The shaded regions were calculated by varying those parameters: $T_{g,org}$ = 313 K (295 K), κ = 0.20 (0.25), D = 13 (10), k_{GT} = 2.5 (3.5) for the upper (lower) limit. Mass loadings were 23 μg m^{-3} for LRH and 8 μg m^{-3} for HRH (Hinks et al., 2017).

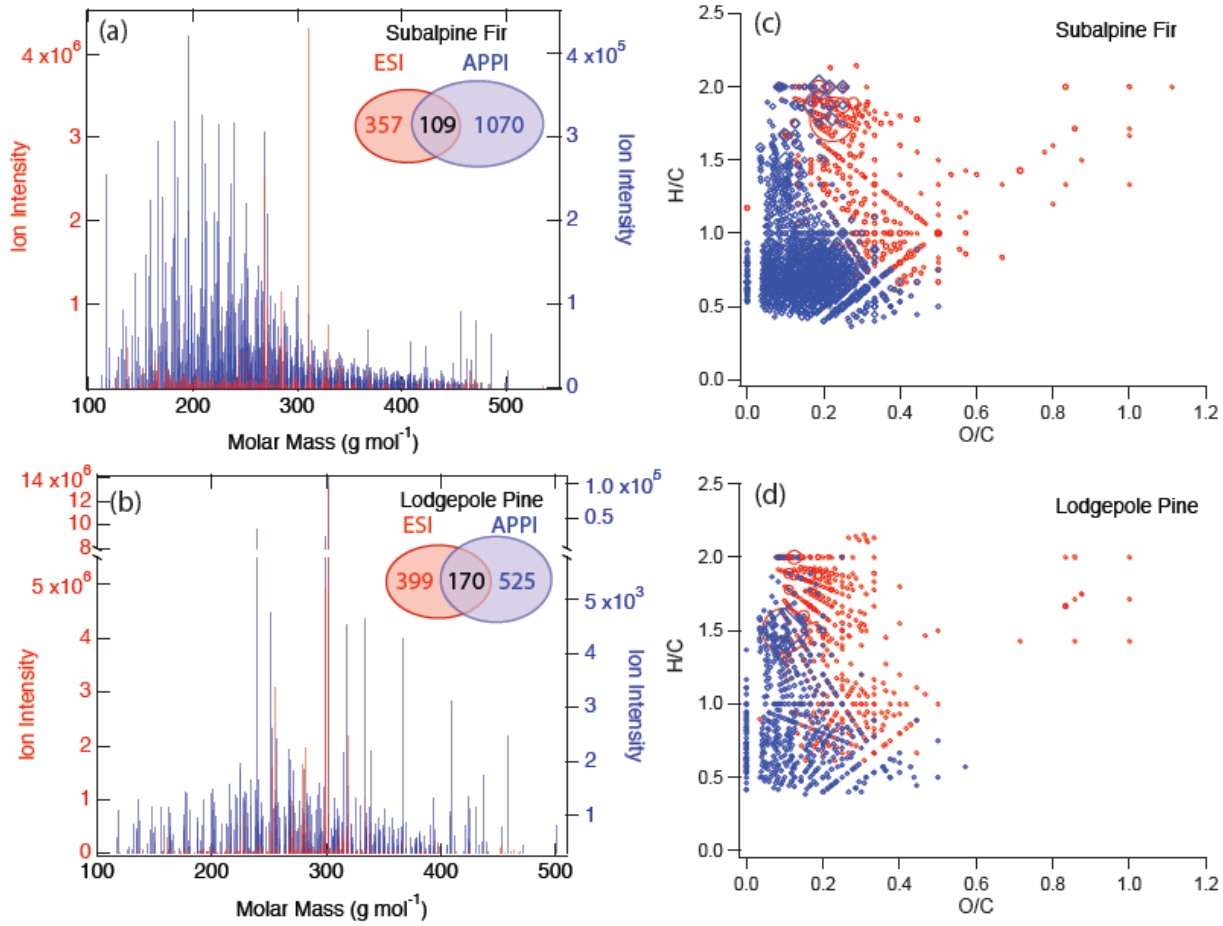

Figure 8. Mass spectra of biomass burning organic particles collected from test burns of (a) subalpine fir and (b) lodgepole pine as measured by high resolution mass spectrometry with two ionization techniques: electron spray ionization (ESI, red) and atmospheric pressure photoionization (APPI; blue). Numbers of elemental formulas identified by ESI (red), APPI (blue) and both modes (black) are also specified. Van Krevelen plots of the compounds identified by ESI (red) and APPI (blue) mode in BBOA from burning of (c) subalpine fir and (d) lodgepole pine.

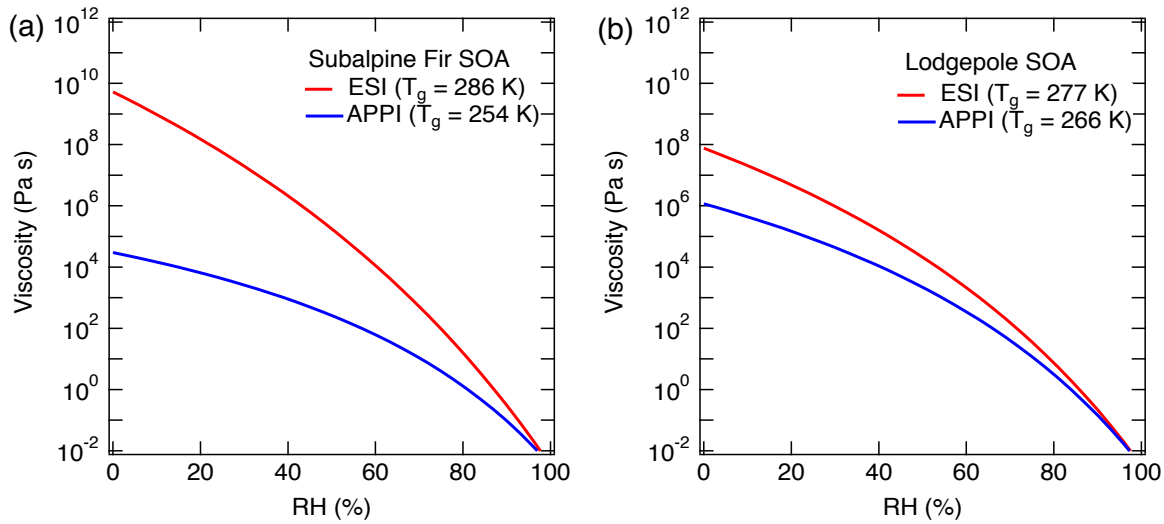

Figure 9. Predicted viscosity for biomass burning particles of (a) subalpine fir and (b) lodgepole pine trees as measured by high resolution mass spectrometry with two ionization techniques: electrospray ionization (ESI, red) and atmospheric pressure photoionization (APPI; blue). $T_{g,org}$ are specified in the figure legend and other used parameters are fixed to $\kappa = 0.1$, $D = 10$, $k_{GT} = 2.5$.

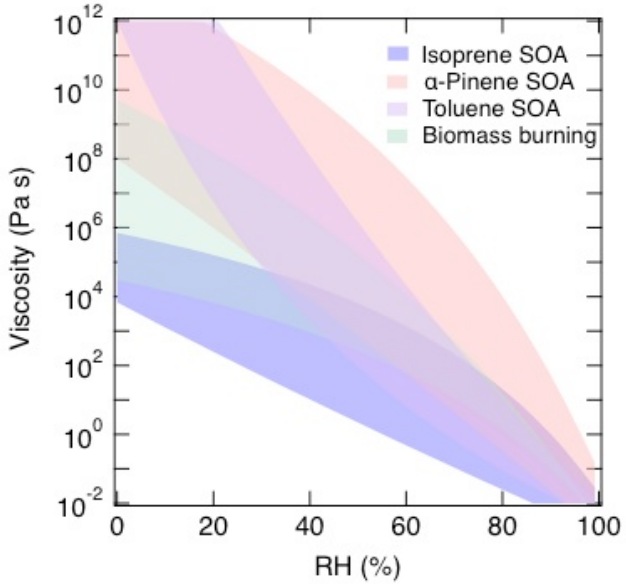

Figure 10. Summary of predicted range of viscosity of α-pinene SOA (red), isoprene SOA (blue), toluene SOA (purple), and biomass burning particles (green).

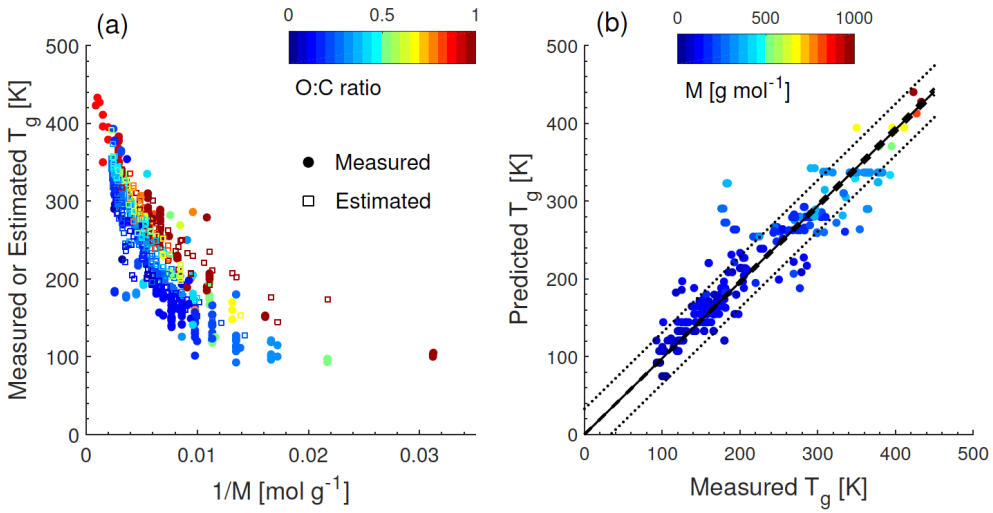

Figure A1. (a) T_g of organic compounds as measured (circles) and estimated with the Boyer-Kauzmann rule (squares) plotted against the inverse molar mass. The markers are color-coded by atomic O:C ratio. (b) Predicted T_g for CHO compounds using a parameterization (Eq. 2) developed in this study compared to measured T_g (circles). The solid line shows 1:1 line and the dashed and dotted lines show 68% confidence and prediction bands, respectively.

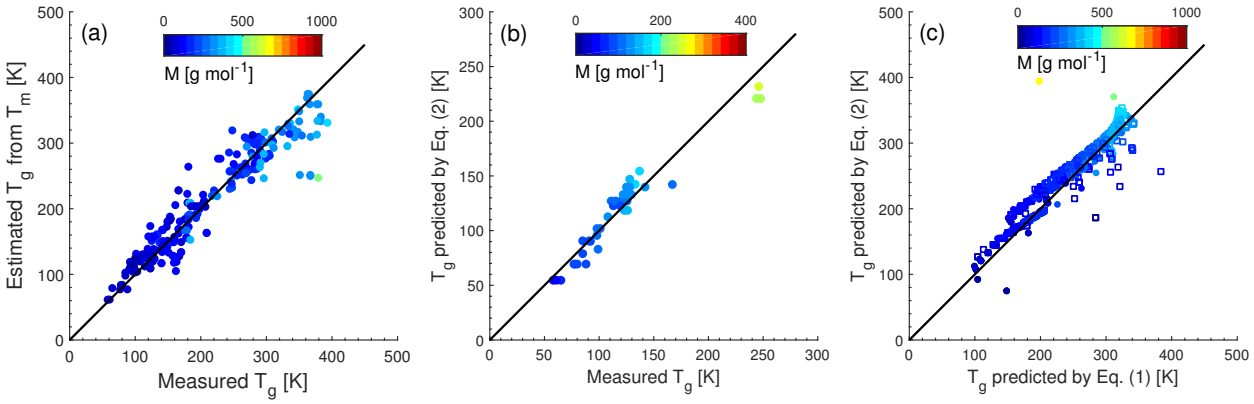

Figure A2. (a) Comparison of measured and estimated T_g by the Boyer-Kauzmann rule for 251 organic compounds (Koop et al., 2011; Dette et al., 2014; Rothfuss and Petters 2017) with their measured T_m available. The markers are color-coded by molar mass. (b, c) Predicted T_g using Eq. (2) compared with (b) measured T_g for CH compounds and (c) predicted T_g using Eq. (1) for CHO compounds. The solid line shows 1:1 line. Solid circle markers represent organic compounds as compiled in Koop et al. (2011) and open square marker represent SOA oxidation products in Shiraiwa et al. (2014) in panel (c).

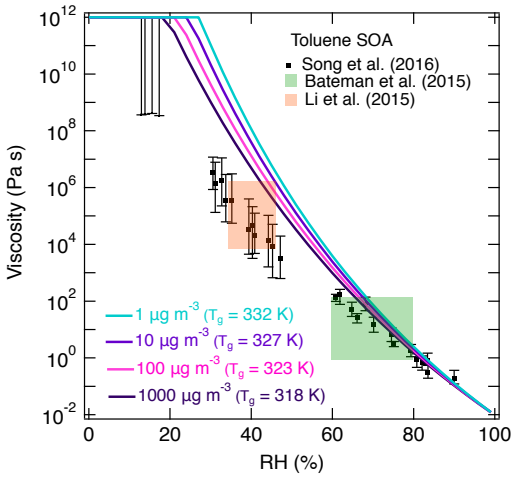

Figure A3. Effect of mass loading on predicted viscosity for toluene SOA. Solid lines represent the predicted viscosity with Eq. (2) using chemical composition of toluene SOA formed at low RH. Viscosity was predicted with different mass loadings ranging from 1-1000 μg m^{-3}. Markers and shaded boxes represent experimentally measured viscosity values. Song et al. (2016) mass loadings were 60-100 and 600-1000 μg m^{-3}. Bateman et al., (2015) and Li et al., (2015) mass loadings were 30-50 μg m^{-3} and 44-125 μg m^{-3}, respectively.